Document Title:	**Investigating Kinetic and Thermodynamic Approaches to Predict Evaporation of Gasoline at Elevated Temperatures for Fire Debris Applications**
Author(s):	**Ruth Smith, Victoria L. Mcguffin, Glen P. Jackson**
Document Number:	**305866**
Date Received:	**February 2023**
Award Number:	**2018-DU-BX-0225**

2022

Investigating Kinetic and Thermodynamic Approaches to Predict Evaporation of Gasoline at Elevated Temperatures for Fire Debris Applications

FINAL RESEARCH REPORT

RUTH SMITH, VICTORIA L. MCGUFFIN, AND GLEN P. JACKSON

This resource was prepared by the author(s) using Federal funds provided by the U.S. Department of Justice. Opinions or points of view expressed are those of the author(s) and do not necessarily reflect the official position or policies of the U.S. Department of Justice.

Federal Award Number: 2018-DU-BX-0225
Project Title: Investigating Kinetic and Thermodynamic Approaches to Predict Evaporation of Gasoline at Elevated Temperatures for Fire Debris Applications

Principal Investigators: Ruth Smith, Ph.D.
Forensic Science Program & Dept. of Chemistry
Michigan State University, East Lansing, MI
rwsmith@msu.edu

Victoria L. McGuffin, Ph.D.
Dept. of Chemistry
Michigan State University, East Lansing, MI
mcguffin@msu.edu

Glen P. Jackson, Ph.D.
Dept. Forensic and Investigative Sciences
West Virginia University, Morgantown, WV
Glen.Jackson@mail.wvu.edu

Recipient Organization: Michigan State University, 426 Auditorium Road, Rm 2
Hannah Administration Building, East Lansing, MI 48824

Project Period: 01/01/2019 – 12/31/2022

Award Amount: $466,769

Table of Contents

Summary of the Project

The goal in forensic fire debris analysis is to identify the chemical class of any ignitable liquid present in debris submitted from the scene of a suspicious fire. Typically, ignitable liquid residue in the submitted debris sample is extracted using one of many available procedures and the extract is analyzed by gas chromatography-mass spectrometry (GC-MS) [1-5]. The resulting total ion chromatogram (TIC) is compared to a reference database containing TICs of ignitable liquids representing the eight chemical classes identified in ASTM E1618 [4]. However, given the complex nature of the submitted samples, there are many challenges in the identification, including, but not limited to, evaporation of the liquid and the presence of substrate interferences.

Any liquid present at the scene is likely to have undergone evaporation due to the high temperatures reached during the fire. As a result, the chemical composition of the liquid changes (*e.g.*, volatile content is reduced or absent) such that the TIC of the evaporated liquid may look quite different from the TIC of the unevaporated liquid. To address this challenge, reference databases often include TICs of experimentally evaporated liquids in addition to the unevaporated counterparts. However, different methods to evaporate the liquid have been documented (*e.g.*, agitation, under nitrogen, different temperatures, *etc.*) and, depending on the volatility of the liquid, evaporation can be a relatively time-consuming process [6-9]. As a result, the reference collection may only include TICs for a relatively small number of evaporated ignitable liquids and may only include a few different evaporation levels for each liquid.

An alternative approach is to model the evaporation process and predict chromatograms corresponding to different levels of evaporation for a given liquid. Numerous models have been reported to predict evaporation of fuels, primarily for environmental applications [10-17]. While the success of such models was demonstrated, there were limitations particularly for forensic applications. Many of the models required that the identity of the liquid in question was known such that the necessary model input property (*e.g.*, boiling point, vapor pressure, *etc.*) could be determined. Further, many of the models predicted evaporation of a single component in the fuel sample, rather than the bulk fuel [11-13, 16, 17].

Previous work by both of our groups focused on developing models to predict evaporation with a focus on forensic applications, albeit using different approaches [18-20]. McGuffin and Smith reported a kinetic-based approach in which the evaporation rate constants of compounds within the liquid sample are predicted as a function of retention index (I^T), which is used a surrogate for boiling point. The advantage in this method is that the identity of the liquid and the compounds within need not be known, only the I^T value at which the compounds elute [19, 20]. Early work demonstrated the accuracy of the model in predicting evaporation of petroleum distillates and gasoline at a range of evaporation levels.

Jackson and co-workers reported a thermodynamic-based approach to predict evaporation of a simulated gasoline sample [18]. Antoine coefficients were used to determine the vapor pressures of compounds in the simulated sample and Raoult's law and Dalton's law were used to calculate the partial and total pressures, respectively. Evaporation was simulated by mathematically subtracting a pre-determined fraction of the vapor phase and re-calculating the partial and total pressures. In the initial work, good agreement between the predicted mole fractions and the relative peak areas of compounds within the simulated sample was demonstrated. Evaporations at high temperatures were simulated and, for equivalent evaporation levels, a higher proportion of volatile compounds remained at high temperatures (500 °C) compared to lower temperatures (25 °C). This apparent discrepancy was attributed to a greater relative increase in the predicted vapor pressures of less volatile compounds at elevated temperatures. As

This resource was prepared by the author(s) using Federal funds provided by the U.S. Department of Justice. Opinions or points of view expressed are those of the author(s) and do not necessarily reflect the official position or policies of the U.S. Department of Justice.

such, at elevated temperatures, there was less relative difference in vapor pressure, with the result that evaporation was more uniform, across the seven compounds in the simulated mixture [18].

While both approaches demonstrated the potential to predict evaporation of complex mixtures for fire debris applications [18, 20], a number of steps are necessary as we work toward developing methods that are implementable in forensic laboratories. First, each model requires some degree of refinement. The kinetic model was developed based on compounds eluting across the range $I^T = 800 – 1200$ [19, 20]. However, gasoline, which is the most common liquid used as an accelerant, contains compounds that elute at $I^T < 800$. As such, there is a need to extend the kinetic model to span the range $I^T = 500 – 1200$ to include the I^T range of compounds in gasoline. Further, given the importance of temperature highlighted by Jackson and co-workers, the extended model should be refined to include a temperature term, thereby generating a variable-temperature kinetic model. For the thermodynamic model, the identity of the liquid in question currently needs to be known such that the corresponding Antoine coefficients can be determined for vapor pressure calculations [18]. And, the performance of the thermodynamic model when applied to more complex mixtures must also be evaluated.

Following refinement of each model, the second step is to conduct a comprehensive evaluation of the kinetic-based and thermodynamic-based approaches to predict evaporation. However, such an evaluation is not yet possible given that the models were developed using different samples, have different inputs and outputs, and use different methods to evaluate predictive accuracy. As such, a comprehensive evaluation of the kinetic-based and thermodynamic-based approaches requires that the models are developed on the same fundamental basis, using the same data set, and using the same metrics for performance comparisons.

Finally, the practical application of the models in a forensic setting must be demonstrated. Although gasoline is the most common ignitable liquid, the ability to predict evaporation of other liquid classes defined by ASTM must be demonstrated [4]. Further, as chromatograms of debris samples typically contain substrate interferences, current practice includes the evaluation of extracted ion profiles (EIPs) of relevant compound classes in addition to the TIC for identification. As such, for practical application, it is also important to demonstrate the ability to predict EIPs for comparison to those of a submitted sample.

To address the afore-mentioned limitations, the four major goals defined in this project were:

- Goal 1: Refine and validate the kinetic-based model to accurately predict evaporation of volatile compounds in gasoline and to include temperature as a variable.
- Goal 2: Refine and validate the thermodynamic-based model to accurately predict evaporation of gasoline.
- Goal 3: Investigate the kinetic and thermodynamic approaches for accurate prediction of gasoline evaporation at temperatures up to 210 °C.
- Goal 4: Demonstrate the application of the kinetic and thermodynamic approaches to identify gasoline at any evaporation level in fire debris samples.

The research design, methods, analytical and data analysis techniques along with the activities and outcomes for each goal are described in the following sections.

Goal 1: Refine and validate the kinetic-based model to accurately predict evaporation of volatile compounds in gasoline and to include temperature as a variable.

The McGuffin and Smith groups previously developed fixed-temperature and variable-temperature kinetic models to predict evaporation rate constants as a function of retention index (I^T) [21]. The models were developed using diesel, a petroleum distillate that contains several compound classes across a range of volatilities. Diesel was evaporated in an evaporation chamber under controlled temperature (5, 10, 20, 30, and 35 °C) and humidity conditions for 300 h. At several time points during the evaporation, samples were removed and analyzed by gas chromatography-mass spectrometry (GC-MS). The abundances of 51 compounds, representing four compound classes in diesel, were normalized to the abundance of C_{21} as an internal standard. For each compound, the normalized abundance was plotted as a function of evaporation time and the first-order kinetic rate equation (Eq. 1) was fit to the decay curves to determine the evaporation rate constant (Fig. 1)

$$C_t = C_0 e^{-kt} \quad \text{Eq. 1}$$

where, C_t and C_0 are concentration at time t and time 0, respectively, k is the evaporation rate constant (h^{-1}) and t is time (h).

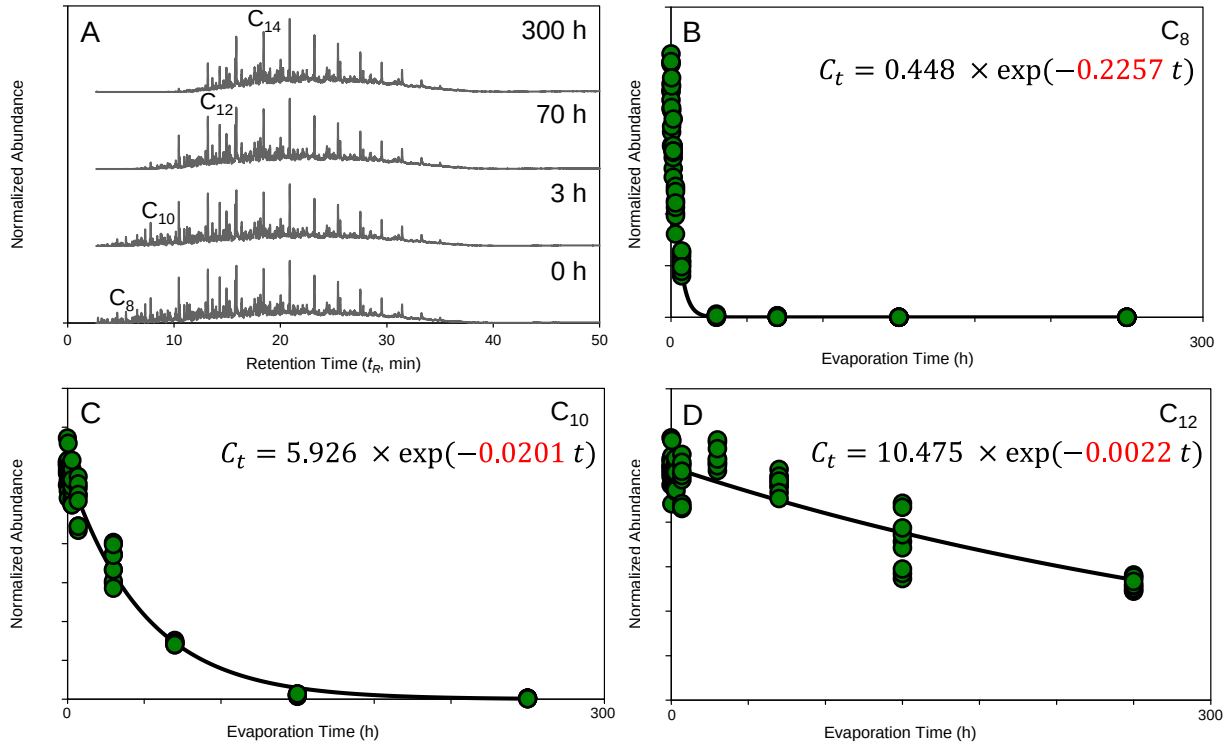

Figure 1. Experimental determination of evaporation rate constants (A) representative total ion chromatograms (TICs) of diesel evaporated at 20 °C for 0, 3, 70, and 300 h and fitting the first-order rate equation to decay curves corresponding to (B) *n*-octane (I^T = 800), (C) *n*-decane (I^T = 1000), and (D) *n*-dodecane (I^T = 1200). In (B – D), decay curves are fit to the first-order rate equation to determine evaporation rate constants (shown in red).

This resource was prepared by the author(s) using Federal funds provided by the U.S. Department of Justice. Opinions or points of view expressed are those of the author(s) and do not necessarily reflect the official position or policies of the U.S. Department of Justice.

For each evaporation temperature, the experimentally determined rate constants were then plotted as a function of I^T (Fig. 2) and linear regression was performed to define the fixed-temperature kinetic models (general form shown in Eq. 2). Multiple linear regression was also performed on the same data to define the variable-temperature kinetic model (general form shown in Eq. 3).

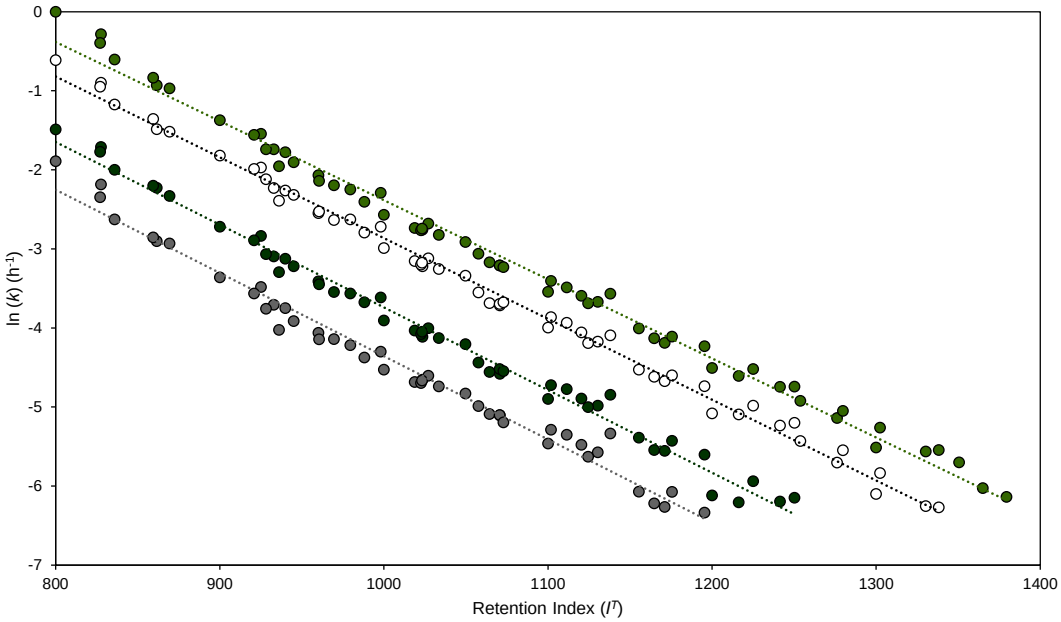

Figure 2. Experimentally determined rate constants plotted as a function of retention index and temperature to define the fixed- and variable-temperature models.

$$ln(k) = m_1 I^T + b \qquad \text{Eq. 2}$$

$$ln(k) = m_1 I^T - m_2 \left(\frac{1}{T}\right) + b \qquad \text{Eq. 3}$$

Predicted rate constants were then be used to generate chromatograms corresponding to any evaporation level of a given liquid. To do so, Eq. 1 is rearranged to express in the form of a fraction remaining (F_{I^T}), as shown in Eq. 4

$$F_{I^T,t} = \frac{C_{I^T,t}}{C_{I^T,0}} = exp(-k\ t) \qquad \text{Eq. 4}$$

where $F_{I^T,t}$ is the fraction remaining of a compound with retention index I^T at time t and $C_{I^T,t}$ and $C_{I^T,0}$ are the concentrations of the same compound at time t and $t = 0$, respectively. To determine $F_{I^T,t}$, Eq. 2 and Eq. 3 are solved for k and then substituted into Eq. 4, yielding Eq. 5 and Eq. 6 for the fixed- and variable-temperature models, respectively.

$$F_{I^T,t} = \frac{C_{I^T,t}}{C_{I^T,0}} = exp(-exp(m_1 I^T + b)\ t) \qquad \text{Eq. 5}$$

This resource was prepared by the author(s) using Federal funds provided by the U.S. Department of Justice. Opinions or points of view expressed are those of the author(s) and do not necessarily reflect the official position or policies of the U.S. Department of Justice.

$$F_{I^T,t} = \frac{C_{I^T,t}}{C_{I^T,0}} = exp\left(-exp\left(m_1 I^T - m_2\left(\frac{1}{T}\right) + b\right)\, t\right) \qquad \text{Eq. 6}$$

The total fraction remaining of a liquid (F_{Total}) is given by Eq. 7

$$F_{Total} = \frac{\sum_{j=I_i^T}^{I_f^T} F_j C_j}{\sum_{j=I_i^T}^{I_f^T} C_j} \qquad \text{Eq. 7}$$

where I_i^T and I_f^T are the initial and final retention indices, respectively across the I^T range of interest, F_j is the fraction remaining of a given compound and C_j is the concentration of the compound, which is proportional to the chromatographic abundance. Predicted chromatograms are generated by multiplying the fraction remaining at a given I^T (F_{I^T}, determined from Eq. 5 or Eq. 6) by the chromatographic abundance at the same I^T in the chromatogram of the unevaporated sample. To generate a chromatogram corresponding to a specific F_{Total} level, t in Eq. 5 or Eq. 6 is varied until the F_{Total} equals the F_{Total} calculated for the experimental chromatogram.

Subsequent work demonstrated successful application of the models to predict evaporation of petroleum distillates and gasoline [20, 22]. However, the kinetic models were developed across the range I^T = 800 – 1200 but gasoline contains a mass of substantially more volatile compounds that elute with I^T < 800. As such, the evaporation rate constants predicted for these more volatile compounds were extrapolated from the original models. Thus, the first goal in the current work was to refine the kinetic models by extending the range to cover I^T = 500 – 1200.

1.1 Research Design and Methods

1.1.1 Identification of compounds of interest

The first step was to identify volatile compounds of interest in gasoline. To do this, unevaporated gasoline was analyzed by GC-MS, turning the detector off only during solvent elution to maximize the number of compounds observed. A total of 15 compounds were initially identify *via* a mass spectral library search and corresponding reference standards for the following 12 compounds were purchased: 2-methylbutane, *n*-pentane, 3-methylpentane, *n*-hexane, methylcyclopentane, 2,3-dimethylpentane, 2-methylhexane, *n*-heptane, 2,2,4-trimethylpentane, methylcyclohexane, toluene, and *n*-octane. The reference standards were subsequently analyzed individually by GC-MS using the same method and identification of the compounds in gasoline was finalized *via* retention time and mass spectral comparison.

Because of the safety concerns associated with the evaporation of gasoline, a series of calculations was performed to determine the volume of vapor (vapor load) that would be expected to be generated by each compound of interest. This step was necessary to ensure that vapor load generated during evaporation in the chamber would not exceed the lower flammability limit (LFL) of the compound. The LFL is the minimum concentration of vapor (% v/v in air) at which flame ignition or explosion is possible in the presence of an ignition source. Based on these calculations, it was determined that binary mixtures of the compounds of interest could be evaporated safely while remaining below the LFL for either compound.

1.1.2 Sample preparation

The binary mixtures were prepared by diluting 0.625 mL of each reference standard and 1 mL of *n*-tridecane (C_{13}, used as an internal standard) to 25 mL with *n*-tetradecane (C_{14}). A validation mixture containing nine compounds (six new compounds and three compounds previously included in model development) was prepared by diluting 2-methylpentane (2 mL), 2,4-dimethylpentane (1 mL), cyclohexane (2 mL), 3-methylhexane (1 mL), *n*-heptane (2 mL), 2,3,4-trimethylpentane (1 mL) toluene (2 mL), cycloheptane (1 mL), and *n*-octane (2 mL) in a mixture of *n*-tridecane (3 mL, internal standard) and *n*-decane (3 mL).

To enable calculation of retention indices, an alkane ladder was also prepared by diluting *n*-pentane, *n*-hexane, *n*-heptane, and *n*-octane in methylene chloride (CH_2Cl_2, all 300:1 v/v).

1.1.3 Experimental evaporations

To perform a given evaporation, a 1-mL aliquot of the binary mixture or validation mixture was placed into 9 separate petri dishes and a further 9 petri dishes were filled with 1-mL aliquots of the C_{14} solvent, which was used as a blank. Each petri dish was placed in the evaporation chamber which was set to the specified evaporation temperature (10, 20, and 30 °C). At nine time points (specific time points varied depending on evaporation temperature) during the evaporation, dishes were removed from the chamber. The evaporations were conducted in duplicate, alternating the time points at which sample and blank petri dishes were removed, such that a full set of time points was collected for each. Upon removal from the chamber, dishes were rinsed with CH_2Cl_2, transferred into separate 5 mL volumetric flasks, and diluted to volume with CH_2Cl_2. An aliquot of the diluted sample was transferred to a GC vial for subsequent analysis.

The validation mixture was evaporated to three different F_{Total} levels at an evaporation temperature of 10 °C and to five different F_{Total} levels at evaporation temperatures of 20 and 30 °C. For each evaporation, 1 mL of the validation mixture was transferred to separate petri dishes, which were then placed into the evaporation chamber. Dishes were removed at time points corresponding to F_{Total} levels in the range 0.3 – 0.8. It is worth nothing that these relatively high F_{Total} levels were necessary to ensure sufficient abundance of the volatile compounds remained to allow an evaluation of the predictive accuracy of the model. Upon removal from the chamber, the evaporated samples were diluted with CH_2Cl_2 (50:1 v/v) and transferred to GC vials for analysis.

1.1.4 GC-MS analysis

All evaporated samples (binary mixtures and blanks) and the alkane ladder were analyzed using an Agilent 6890N gas chromatograph coupled to an Agilent 5975C mass spectrometer and equipped with an Agilent 7683A autosampler (all Agilent Technologies, Santa Clara, CA). The GC contained a non-polar column (100% dimethylpolysiloxane, 30 m x 0.25 mm id, 0.25 µm, Agilent Technologies). The injector temperature was 250 °C, a 1-µL aliquot of sample was injected in pulsed-split mode (15 psi for 0.25 min, 50:1 split), and ultra-high purity helium was used as the carrier gas with a nominal flow rate of 1 mL/min. The oven temperature program was as follows: 35 °C, then 5 °C/min ramp to 175 °C. The transfer line was maintained at 280 °C. Mass spectra were collected in electron ionization (EI) mode at 70 eV, with a scan rate of 2.83 scan/s across the *m/z* range 40-550. The ion source temperature was 230 °C and the quadrupole mass analyzer was held at 150 °C. To allow detection of volatile compounds, no solvent delay was used but instead, the detector was switched off during elution of the CH_2Cl_2 solvent (1.62 – 1.80 min).

1.1.5 Data analysis

Chromatograms of the alkane ladder and each evaporated sample were exported from the instrument software (ChemStation, version E.01.00.237, Agilent Technologies) into Microsoft Excel (version 16.20, Microsoft Corp., Redmond, WA) for further processing.

Retention indices for each compound were calculated using Eq. 8

$$I^T = 100\left[\frac{t^T_{R,i} - t^T_{R,z}}{t^T_{R,z+1} - t^T_{R,z}} + z\right] \qquad \text{Eq. 8}$$

where $t^T_{R,i}$ is the retention time of the compound of interest and $t^T_{R,z}$ and $t^T_{R,z+1}$ are the retention times of the *n*-alkanes with carbon number, *z*, eluting before and after the compound of interest, respectively. In a given chromatogram, the peak abundance for the compound of interest was normalized to the peak abundance of the internal standard. The normalized peak abundances for the compound were then plotted as a function of evaporation time to generate the decay curve. The data were fitted to the first-order rate equation (TableCurve 2D, version 5.01, Jandel Scientific, San Rafael, CA) to determine the evaporation rate constant (*k*) for each compound.

Given the volatility of the compounds of interest, the experimental rate constants were corrected for condensation. To do this, for a given evaporation, the abundance of the compounds of interest in the blank dishes were also normalized and plotted as a function of evaporation time. These data were fit to the first-order rate equation, this time determining *k'*, which is the rate constant for condensation. Corrected rate constants were generated by subtracting the *k'* from *k* for the compound of interest.

For a given evaporation temperature, the corrected rate constants were combined with those previously determined by McIlroy *et al.* for compounds eluting in the range I^T = 800 – 1200 [19]. The natural logarithms of *k* were plotted as a function of I^T and linear regression was performed to define the kinetic model at that temperature (general form shown in Eq. 2), now over the I^T = 500 – 800. The same data (natural logarithm of *k* at each temperature) were combined and multiple linear regression was performed to define the variable-temperature model (general form shown in Eq. 3).

1.1.6 Validation of kinetic models

The kinetic models were used to predict chromatograms corresponding to each F_{Total} level of the validation mixture. The actual F_{Total} for each evaporated validation mixture was calculated by dividing the area under the chromatogram of the evaporated sample by the area under the chromatogram of the unevaporated validation mixture. The kinetic model was then used to predict a chromatogram of the validation mixture corresponding to the same F_{Total} level. To do this, *t* was varied in Eq. 5 (for the fixed-temperature model) and in Eq. 6 (for the variable-temperature model) until the F_{Total} in the predicted chromatogram was equal to that calculated for the validation mixture. The predicted and experimental chromatograms were then evaluated in two ways. First, the percent error (*E*) in abundance of each compound in the predicted and experimental chromatograms was calculated using Eq. 9,

$$E = \frac{A_{I^T,pred} - A_{I^T,exp}}{A_{I^T,exp}} \times 100\% \qquad \text{Eq. 9}$$

where $A_{I^T,pred}$ and $A_{I^T,exp}$ are the chromatographic abundance of a compound with retention index I^T in the predicted and experimental chromatograms, respectively. In these error calculations, the sign indicates

model overprediction (positive error) or underprediction (negative error) for each compound. The mean absolute percent error (MAPE) was also calculated to evaluate model performance in predicting all validation compounds using Eq. 10

$$\bar{E} = \frac{\sum_1^n \left| \frac{A_{I^T,pred} - A_{I^T,exp}}{A_{I^T,exp}} \right|}{n} \times 100\% \qquad \text{Eq. 10}$$

where n is the total number of compounds in the validation mixture.

The predictive accuracy of the model was also evaluated based on the correlation between the predicted and experimental chromatograms. Pearson product-moment correlation (PPMC) coefficients, r, were calculated across the range I^T = 500 – 800 using Eq. 11

$$r = \frac{\Sigma\left[\left(A_{I^T,pred} - \bar{A}_{pred}\right)\left(A_{I^T,exp} - \bar{A}_{exp}\right)\right]}{\sqrt{\Sigma\left(A_{I^T,pred} - \bar{A}_{pred}\right)^2 \Sigma\left(A_{I^T,exp} - \bar{A}_{exp}\right)^2}} \quad \text{Eq. 11}$$

where $A_{I^T,pred}$ and $A_{I^T,exp}$ are the predicted and experimental abundances, respectively, at each I^T value and $\bar{A}_{pred}$ and $\bar{A}_{exp}$ are the average predicted and experimental abundances, respectively. PPMC coefficients range from -1 to +1 with the sign indicating positive or negative correlation. The strength of the association is defined as follows: $|r| \geq 0.8$ indicates strong correlation, $0.79 > |r| \geq 0.5$ indicates moderate correlation, $|r| < 0.49$ indicates weak correlation, and $|r|$ close to zero indicates no correlation [23].

1.2 Results and Findings

1.2.1 Development of fixed- and variable-temperature kinetic models

A representative chromatogram of an unevaporated gasoline sample is shown in Fig. 3A. Volatile compounds that eluted before toluene (highlighted in red box in Fig. 3A) were identified and retention indices were calculated (Table 1). Evaporation rate constants for the compounds of interest were experimentally determined by fitting the decay curves for the individual compounds to the first-order rate equation (Eq. 1), as illustrated in Fig. 3B – D for 2,3-dimethylpentane (I^T = 661), methylcyclohexane (I^T = 716), and *n*-octane (I^T = 800), respectively. A summary of the experimentally determined rate constants, corrected for condensation, at each evaporation temperature is shown in Table 1.

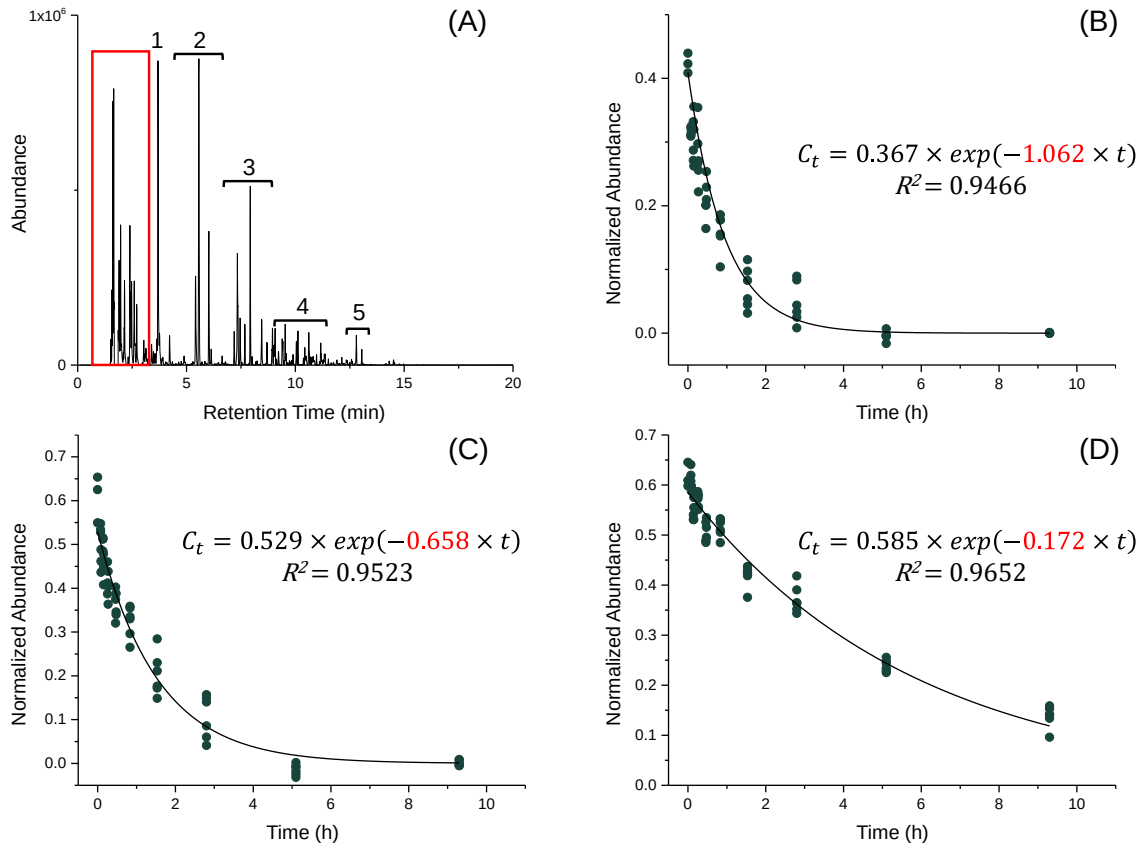

Figure 3. Experimental determination of evaporation rate constants (A) chromatogram of unevaporated gasoline with volatile compounds of interest highlighted in red box, (B) decay curve for 2,3-dimethylpentane (I^T = 661) fit to first-order rate equation, (C) decay curve for methylcyclohexane (I^T = 716), and (D) decay curve for n-octane (I^T = 800). In (A), characteristic gasoline compounds are labeled as follows: (1) toluene, (2) C_2-alkylbenzenes, (3) C_3-alkylbenzenes, (4) C_4-alkylbenzenes, and (5) methylnaphthalenes. In (B – D), decay curves are fit to the first-order rate equation to determine evaporation rate constants (shown in red).

This resource was prepared by the author(s) using Federal funds provided by the U.S. Department of Justice. Opinions or points of view expressed are those of the author(s) and do not necessarily reflect the official position or policies of the U.S. Department of Justice.

Table 1. Corrected evaporation rate constants experimentally determined at 10 °C, 20 °C, and 30 °C

Compound	Retention Index (I^T)	Corrected Evaporation Rate Constant (k, h^{-1})		
		10 °C	20 °C	30 °C
2-Methylbutane	487	17.96	23.46	32.14
n-Pentane	500	5.713	18.56	33.09
3-Methylpentane	578	2.831	4.287	5.805
n-Hexane	600	3.010	3.863	4.731
Methylcyclopentane	621	2.552	2.975	4.037
2-Methylhexane	659	1.105	0.749	2.145
2,3-Dimethylpentane	661	1.062	1.413	2.095
2,2,4-Trimethylpentane	686	0.751	1.011	1.507
n-Heptane	700	0.625	0.823	1.476
Methylcyclohexane	716	0.658	0.749	1.275
Toluene	747	0.521	0.644	1.093
n-Octane	800	0.172	0.240	0.416

The calculated rate constants were combined with rate constants previously calculated by McIlroy *et al.* [19] for compounds eluting in the range I^T = 800 – 1200 at the corresponding temperatures (Fig. 4).

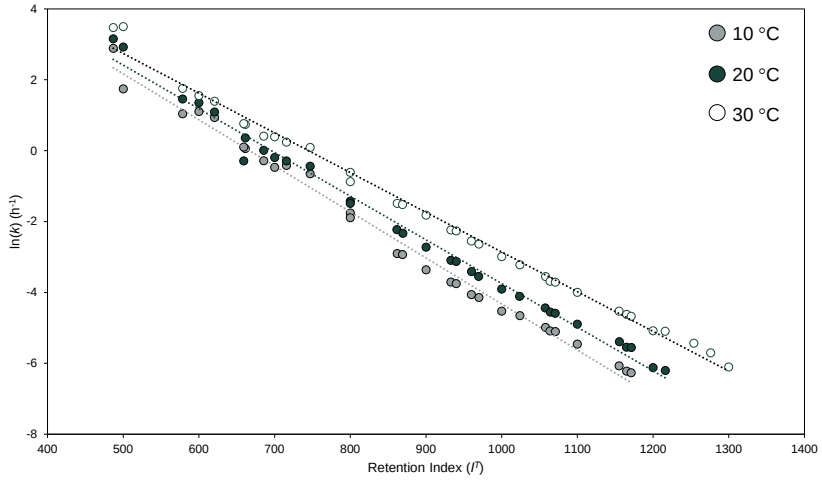

Figure 4. Evaporation rate constants (k) plotted as a function of retention index (I^T) for compounds eluting across the range I^T = 500 – 1200 at 10, 20, and 30 °C.

The natural logarithm of the rate constant was then plotted as a function of I^T and linear regression was performed to define fixed-temperature kinetic models at 10, 20, and 30 °C (Eqs. 12, 13, and 14, respectively).

$$ln(k) = -1.22 \times 10^{-2} I^T + 8.07 \qquad \text{Eq. 12}$$
$$ln(k) = -1.16 \times 10^{-2} I^T + 7.99 \qquad \text{Eq. 13}$$
$$ln(k) = -1.07 \times 10^{-2} I^T + 7.97 \qquad \text{Eq. 14}$$

Multiple linear regression was then performed on the same data (Fig. 4) to define the variable-temperature kinetic model (Eq. 15)

This resource was prepared by the author(s) using Federal funds provided by the U.S. Department of Justice. Opinions or points of view expressed are those of the author(s) and do not necessarily reflect the official position or policies of the U.S. Department of Justice.

$$ln(k) = -1.14 \times 10^{-2} I^T - 6021\left(\frac{1}{T}\right) + 28.5 \quad \text{Eq. 15}$$

1.2.2 Validation of fixed-temperature models

Representative chromatograms of the validation mixture evaporated to different levels at 10 °C are shown in Fig. 5 and overlaid with the corresponding chromatogram predicted using the kinetic model (Eq. 12). The PPMC coefficients for comparison of the predicted and experimental chromatograms are shown in Table 2, along with the mean absolute percent error in predicting abundance of select compounds.

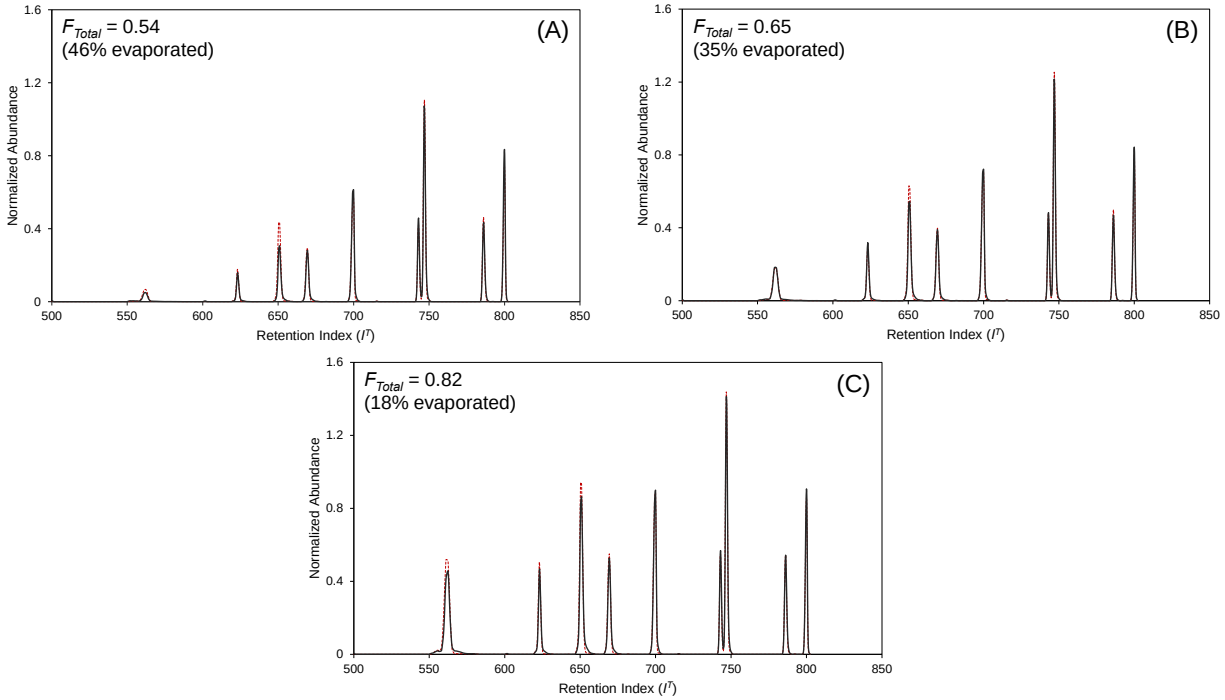

Figure 5. Representative chromatograms of predicted (red dotted line) and experimental (black solid line) chromatograms for a nine-component validation mixture at F_{Total} levels of (A) 0.54, (B) 0.65, and (C) 0.82. Evaporations were conducted at 10 °C.

This resource was prepared by the author(s) using Federal funds provided by the U.S. Department of Justice. Opinions or points of view expressed are those of the author(s) and do not necessarily reflect the official position or policies of the U.S. Department of Justice.

Table 2. Predictive accuracy of the original and refined fixed-temperature models for the validation mixture at 10, 20, and 30 °C

Temperature (°C)	F_{Total}	Original Fixed-Temperature Model[1]		Refined Fixed-Temperature Models[2]	
		PPMC	MAPE (%)	PPMC	MAPE (%)
10	0.54	0.9892	19.1	0.9919	11.2
	0.65	0.9962	6.47	0.9968	7.62
	0.82	0.9936	7.43	0.9948	4.88
20	0.36	0.9801	15.5*	0.9799	17.1*
	0.42	0.9884	11.9*	0.9884	13.5*
	0.53	0.9871	8.68*	0.9868	13.3*
	0.66	0.9958	5.92*	0.9954	8.26*
	0.81	0.9960	8.88	0.9963	7.93
30	0.25	0.9550	24.7*	0.9553	26.4*
	0.36	0.9640	18.1*	0.9640	18.8*
	0.55	0.9836	10.5	0.9835	12.3
	0.69	0.9971	4.90	0.9970	5.81
	0.83	0.9952	4.61	0.9952	4.89

PPMC = Pearson product-moment correlation coefficient

MAPE = mean absolute percent error

[1]Original fixed-temperature models:

10 °C: $\ln(k) = -1.05 \times 10^{-2} I^T + 6.17$

20 °C: $\ln(k) = -1.05 \times 10^{-2} I^T + 6.71$

30 °C: $\ln(k) = -1.02 \times 10^{-2} I^T + 7.35$

[2]Refined fixed-temperature models:

10 °C: $\ln(k) = -1.22 \times 10^{-2} I^T + 8.07$

20 °C: $\ln(k) = -1.16 \times 10^{-2} I^T + 7.99$

30 °C: $\ln(k) = -1.07 \times 10^{-2} I^T + 7.97$

* Normalized abundance of 2-methylpentane less than 5% abundance in chromatogram of unevaporated mixture, so error omitted from MAPE calculation

For the refined kinetic model at 10 °C, PPMC coefficients were greater than 0.99 for comparison of predicted and experimental chromatograms at the three F_{Total} levels, which indicates strong correlation. Further, the mean absolute error in prediction ranged from 4.88% to 11.2% as F_{Total} level decreased from 0.82 to 0.54, which corresponds to an increase in evaporation level from 18 to 46%. Chromatograms corresponding to the same F_{Total} levels were also predicted using the original kinetic model at 10 °C and compared to the corresponding experimental chromatograms (Table 2). For each F_{Total} level, PPMC coefficients were comparable using the original and the refined kinetic models. In terms of prediction errors, the refined model offered improved prediction accuracy for F_{Total} levels corresponding to 0.54 and 0.82 (Table 2). At $F_{Total} = 0.65$, the prediction errors were more comparable between the two models: 6.47% for the original model and 7.62% for the refined model. However, the larger error for the refined model was primarily due to the larger error associated with the prediction of the two most volatile compounds in the mixture: 2-methylpentane ($I^T = 563$) and 2,4-dimethylpentane ($I^T = 623$). When these two compounds were omitted from the error calculations, the errors in prediction were 5.55% and 4.83% for the original and refined models, which indicates improved performance for the latter model.

Similar methods were used to evaluate the performances of the fixed-temperature models at 20 °C (Eq. 13) and 30 °C (Eq. 14) in comparison to the corresponding original models (Table 2). At the higher temperatures, lower F_{Total} levels were evaluated; however, at these levels, the more volatile compounds in

This resource was prepared by the author(s) using Federal funds provided by the U.S. Department of Justice. Opinions or points of view expressed are those of the author(s) and do not necessarily reflect the official position or policies of the U.S. Department of Justice.

the mixture were present at low abundance, resulting in substantially higher errors in prediction. As such, any compound present at less than 5% of the normalized abundance in the chromatogram of the unevaporated mixture was excluded from the MAPE calculation. At each temperature and each F_{Total} level, PPMC coefficients were generally greater than 0.989 and were comparable for the original and refined models. In terms of the MAPE calculations, errors were higher at lower F_{Total} levels for both the original and the refined models, primarily due to lower abundances in the chromatogram due to the greater extent of evaporation. While the MAPE values were slightly lower for the original models compared to the refined models, the average difference in error was only 2.2% and 1.1% at 20 °C and 30 °C, respectively. Overall, these results indicate comparable performance of the original and the refined fixed-temperature models across three evaporation temperatures and up to five F_{Total} levels.

1.2.3 Validation of variable-temperature model

The variable-temperature model defined by McIlroy *et al.* was developed based on evaporations at five temperatures ranging from 5 – 35 °C. In the current work, evaporations were conducted at three temperatures (10, 20, and 30 °C). To enable direct comparison of the original and refined variable-temperature models, the original model was re-defined based on rate constants determined at 10, 20, and 30 °C (*i.e.*, rate constants determined at 5 °C and 35 °C were excluded from the multiple linear regression analysis used to define the model). The original model was re-defined according to Eq. 16

$$ln(k) = -1.03 \times 10^{-2} I^T - 6444\left(\frac{1}{T}\right) + 28.7 \qquad \text{Eq. 16}$$

The re-defined original model (Eq. 16) and the refined model developed in this work (Eq. 15) were used to predict chromatograms corresponding to the evaporated validation mixture at each temperature, following procedures described in Section 1.2.2 (Table 3).

At 10 °C, the refined variable-temperature model offered slightly higher PPMC coefficients and lower errors in predicting compound abundances. However, at 20 and 30 °C, while PPMC coefficients were comparable between the original and refined models, the former model resulted in lower prediction errors. The MAPE values represent an average error in prediction across all compounds. When errors in prediction of individual compounds are considered, the refined models offered improved prediction of certain compounds (*e.g.*, 2,3,4-trimethylpentane and n-octane) but poorer prediction of other compounds (*e.g.*, 2-methylpentane and 2,4-methylpentane) compared to the original models. The higher prediction errors for the two most volatile compounds require further investigation given that the refined model now extends to include the I^T range in which these compounds elute. Despite this, it is worth noting that the original and refined models offer comparable predictive performance and that the refined model now extends into an I^T range for which evaporation rate constants had not been measured previously.

Table 3. Predictive accuracy of the original and refined variable-temperature models for the validation mixture at 10, 20, and 30 °C

Temperature (°C)	F_{Total}	Original Variable-Temperature Model[1]		Refined Variable-Temperature Model[2]	
		PPMC	MAPE (%)	PPMC	MAPE (%)
10	0.54	0.9887	23.4	0.9908	13.9
	0.65	0.9961	7.07	0.9967	5.42
	0.82	0.9933	6.72	0.9943	5.34
20	0.36	0.9800	15.3*	0.9800	16.9*
	0.42	0.9884	11.8*	0.9885	13.3*
	0.53	0.9870	8.19	0.9869	12.6
	0.66	0.9958	5.79	0.9955	7.89
	0.81	0.9960	8.94	0.9962	8.08
30	0.25	0.9551	24.8*	0.9554	31.4*
	0.36	0.9640	18.2*	0.9638	19.6*
	0.55	0.9836	10.8	0.9833	14.6
	0.69	0.9971	5.06	0.9967	7.05
	0.83	0.9952	4.73	0.9950	5.30

PPMC = Pearson product-moment correlation coefficient
MAPE = mean absolute percent error
[1]Original variable-temperature model: $\ln(k) = -1.03 \times 10^{-2} I^T - 6444\,(1/T) + 28.7$
[2]Refined variable-temperature model: $\ln(k) = -1.14 \times 10^{-2} I^T - 6021\,(1/T) + 28.5$
* Normalized abundance of 2-methylpentane less than 5% abundance in chromatogram of unevaporated mixture, so error omitted from MAPE calculation

1.3 Activities and Accomplishments

Peer-reviewed publications

Burkhart AL, Waddell Smith R, McGuffin VL. Measuring Evaporation Rate Constants of Highly Volatile Compounds for Use in Predictive Kinetic Models. *Analytica Chimica Acta* 1182, **2021**, 338932. https://doi.org/10.1016/j.aca.2021.338932.

*Conference presentations (presenting author underlined, † indicates graduate student, †† indicates undergraduate student, * indicates invited presentation)*

†Amanda L. Setser, Victoria L. McGuffin, and Ruth Waddell Smith. Refinement and Application of a Kinetic Model to Predict Evaporation of Gasoline for Fire Debris Analysis. Oral presentation at the 72nd American Academy of Forensic Sciences Annual Meeting, Anaheim, CA. February 2020.

*†Amanda L. (Setser) Burkhart, Victoria L. McGuffin, and Ruth Waddell Smith. Predicting Evaporation of Volatile Compounds in Gasoline using a Refined Kinetic Model. Oral presentation at the 72nd Annual Pittsburgh Conference on Analytical Chemistry and Applied Spectroscopy (Pittcon, virtual). March 2021.

Theses

Burkhart, AL. Measuring Evaporation Rate Constants of Highly Volatile Compounds and Investigating the Effect of Interface on a Kinetic Model Applied to Forensic Fire Debris. PhD Thesis, **2021**, Michigan State University, East Lansing, MI.

1.4 Limitations and Areas of Future Work

In this goal, evaporation rate constants of volatile compounds eluting in the range I^T = 500 – 800 were measured experimentally and combined with rate constants previously determined over the range I^T = 800 – 1200 to develop fixed- and variable-temperature models. Throughout this work, evaporations were conducted at low temperatures (10 – 30 °C); however, given that fires will burn at substantially higher temperatures, evaporation rate constants should be experimentally determined at higher temperatures to develop additional kinetic models. The current kinetic models were developed based on evaporation rate constants of compounds representing four distinct chemical classes (*n*-alkanes, branched alkanes, alkyl benzenes, and polycyclic hydrocarbons). Moving forward, evaporation rate constants for compounds representing additional compound classes (*e.g.*, oxygenated compounds) will be determined and included in model development to define even more comprehensive models.

Goal 2: Refine and validate the thermodynamic-based model to accurately predict evaporation of gasoline.

To accomplish this goal, and to simplify the experiments and calculations, refinement and validation of the thermodynamic model were first conducted on a nine-component mixture before extending the work to actual gasoline. Details of the accomplishments towards this goal are described in *Forensic Chemistry* [24]. The work is summarized below. **Figure 6** provides a graphical summary of the work, which is that our model accurately fits the experimental data, and that liquids weathered to a particular extent at an elevated temperature of, say, 210 °C will contain more volatiles than the same liquid weathered to the same extent at near-room temperature.

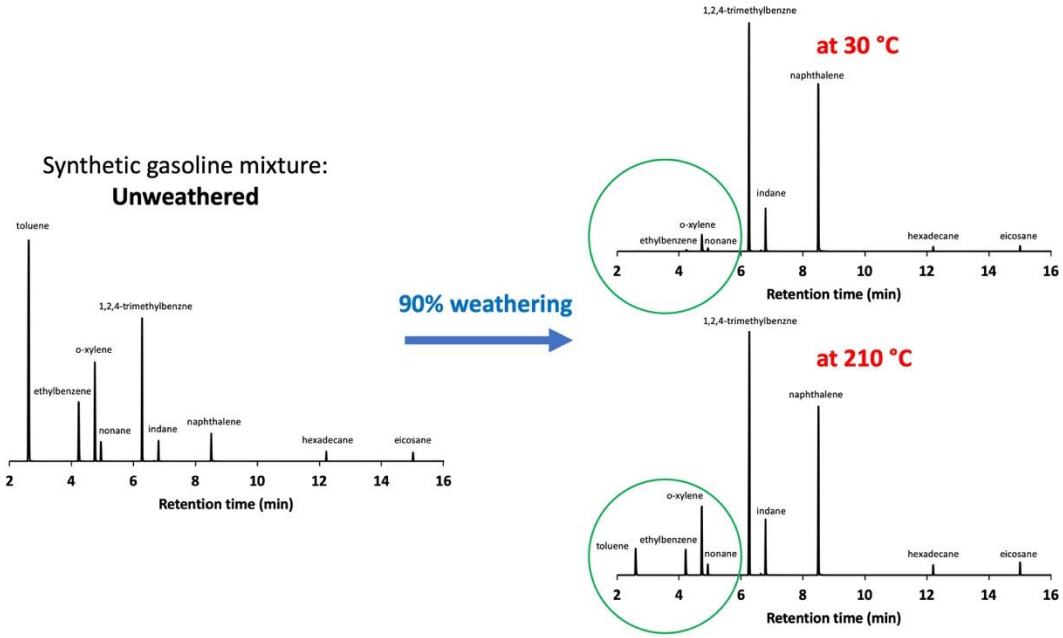

Figure 6. Gas chromatograms to show how weathering at elevated temperatures (*e.g.*, 210 °C) provides in residues with a larger proportion of volatiles than weathering close to room temperature.

2.1 Research Design and Methods

The relative quantities of nine compounds were first measured in an unweathered commercial gasoline sample (Kroger, Morgantown, WV, USA) by dissolving the commercial gasoline 1:200 in pentane and analyzing the diluted sample in triplicate using GC/MS (see GC/MS section for details). In the commercial unweathered gasoline sample, hexadecane and eicosane were below the detection limits, so the concentration of these two compounds was artificially elevated in the artificial gasoline recipe to ensure that they were always quantifiable. The inclusion of compounds with boiling points up to nC_{20} provides greater confidence that the model will be applicable to a wide range of ignitable liquids and not just gasoline.

A 200-mL stock solution of the artificial gasoline was prepared, and 1-mL aliquots of this stock solution were weathered to different extents at different temperatures (30, 90, 150, and 210 °C), as described below. The relative total ion chromatogram (TIC) peaks areas of the final artificial gasoline recipe were toluene (46.6%), ethylbenzene (9.3%), *o*-xylene (15.0%), nonane (2.8%), 1,2,4-trimethylbenzene

This resource was prepared by the author(s) using Federal funds provided by the U.S. Department of Justice. Opinions or points of view expressed are those of the author(s) and do not necessarily reflect the official position or policies of the U.S. Department of Justice.

(19.7%), indane (2.8%), naphthalene (3.8%), hexadecane (0.06%) and eicosane (0.05%). The theoretical basis of the model uses fractional molar ratios and the simulations are based on fractional GC peak areas; these fractions are modestly different in proportion to the relative sensitivity factors of each component quantified by the GC/MS. However, we have verified that, from a mathematical perspective, there is no significant difference between simply modeling GC peak areas directly and the cumbersome alternative, which would require first converting peak areas to molar ratios, then modeling the change in molar ratios before converting the molar ratios back to peak areas.

2.1.1. Weathered Artificial Gasoline Sample Preparations

Replicate 1 mL aliquots of the artificial gasoline sample were weathered at four different temperatures (30, 90, 150, and 210 °C) to various percentages (50-99%). By necessity, the extent of weathering was determined by mass, not volume, so the mass of the initial liquid and the mass of the residue were assessed differently. The initial mass of the liquid was established from the starting volumes of 1 mL and the measured density. The average density of the artificial gasoline was established to be 0.853 g/mL by weighing five replicate aliquots of 1 mL transfers.

Weathering was conducted in aluminum weigh boats that were heated to 400 °C in a kiln (Paragon Digital High Fire Kiln, Paragon Industries Inc., Sapulpa, OK, USA) to remove residual organic lubricants and contaminants. The empty weigh boats were weighed and countersunk in a custom-made aluminum block, and both were pre-heated to the desired weathering temperature in a standard oven (Lindberg Blue M, Thermo Scientific, Waltham, MA, USA) before each weathering experiment. Once at the desired temperature, the hot block and weigh boat were transferred to a fume hood and 1 mL (0.853 g) of the artificial gasoline sample was spiked onto the hot weight boat. After reaching the desired extent of weathering, the weigh boat was transferred to a replicate aluminum block that was previously cooled to -20 °C in a freezer. The cold block immediately cooled the weigh boat and its residues thereby minimizing the weathering process.

After weighing the weigh boat and its residues to quantify the extent of evaporation, the weigh boat was washed with five successive washes of 0.5 mL of pentane. The washings were transferred to a GC vial where they were combined. Because the pentane evaporates so quickly during the washing steps, the five combined replicates typically provided a total volume between 0.6-1 mL of washings. The weigh boats were weighed after the five replicate washes to ensure that all the residues were collected. The dissolved residues were then brought to a final volume of 1 mL. Because each weathering experiment resulted in a different mass of residue in the 1 mL of pentane washings, different volumes of each washing were subsequently diluted to provide final working solutions that were all 1:200 of weathered residue in pentane.

2.1.2. Gas Chromatography-Mass Spectrometry

All samples were analyzed using an Agilent Technologies 7890B GC/5977A MS with a 30 m x 250 µm x 0.25 µm film thickness HP-5 column (Agilent J&W Columns). The GC/MS parameters were as follows: 0.5 µL injection volume; 250 °C injection temperature; 20:1 split ratio; the initial oven temperature was 40 °C (3.0 min hold), which was ramped to 250 °C at 15 °C/min (3.0 min hold) and then ramped to 280 °C at 10 °C/min (3.0 min hold). The total run time for the GC/MS analysis was therefore 26.50 minutes. The carrier gas was ultra-high purity helium (Matheson, Fairmont, WV, USA) with a flow rate of 1 mL/min. The mass spectrometer was scanned from *m/z* 40-350 at a scan rate was 781 Da/sec after a 1.50 min solvent delay. The transfer line and ion source temperatures were 270 °C and 250 °C, respectively. A

pentane blank and an n-alkane ladder were run with all samples. The resulting data was extracted and analyzed using Microsoft Excel version 15 (Microsoft Corporation, Redmond, WA, USA).

2.1.3. Iterative Evaporation Model

The simple mathematical model employs iterative fractional losses (e.g., 5% each step) of the mixture components in proportion to their theoretical partial pressures. The partial pressures of the constituents are determined using either: 1) Raoult's law and Antoine constants from the literature, or 2) Henry's law. Table 4 shows the predicted vapor pressures for each pure compound at 30, 90, 150, 210, and 500 °C [25]. These vapor pressures were predicted using well-characterized Antoine coefficients. The Antoine coefficients are most accurate within certain established temperature ranges [25], and because the present model estimates vapor pressures outside of some of these well-defined regions, the calculated vapor pressures contain a certain degree of error. However, the magnitude of these uncertainties is expected to be negligible relative to the orders-of-magnitude changes in the absolute vapor pressures at the different temperatures.

Table 4. Retention times and calculated vapor pressures of each compound in the artificial gasoline mixture (bar)

Temperature (°C)	Toluene	Ethyl-benzene	*o*-Xylene	Nonane	1,2,4-TMB	Indane	Naphthalene	Hexadecane	Eicosane
t_R (min)	2.62	4.24	4.76	4.95	6.28	6.81	8.51	12.22	15.05
30	5.0E-02	1.8E-02	1.2E-02	8.8E-03	4.4E-03	3.0E-03	1.6E-04	3.4E-06	4.9E-08
90	5.4E-01	2.4E-01	1.8E-01	1.5E-01	8.2E-02	6.2E-02	1.1E-02	5.5E-04	3.3E-05
150	2.8E+00	1.5E+00	1.2E+00	9.9E-01	6.0E-01	4.8E-01	1.4E-01	1.4E-02	1.8E-03
210	9.2E+00	5.3E+00	4.5E+00	3.9E+00	2.6E+00	2.1E+00	8.3E-01	1.3E-01	2.6E-02
500	1.9E+02	1.4E+02	1.3E+02	1.2E+02	1.0E+02	8.5E+01	5.0E+01	2.6E+01	1.1E+01

Toluene is the earliest eluting compound in the artificial gasoline and possesses the highest vapor pressure of 5.0×10^{-2} bar at 30 °C. Eicosane is the latest eluting compound and has the lowest vapor pressure of 4.9×10^{-8} bar at 30 °C. At 30 °C, their vapor pressures are different by six orders of magnitude. The vapor pressure increases with temperature for all compounds, but the magnitude of the increase is greatest for the latest eluting compounds. For example, at 210 °C, toluene has a vapor pressure of 9.2 bar whereas the vapor pressure for eicosane is 2.6×10^{-2} bar. Therefore, at 210 °C, toluene and eicosane are only different by a little more than two orders of magnitude. The range in vapor pressures of all the compounds is significantly smaller at elevated temperatures than at room temperature, and this similarity at elevated temperatures explains why the compounds evaporate at more similar rates at elevated temperatures relative to room temperature.

2.2 Results and Findings

2.2.1 Mathematical Simulations

The simulations are based on sequential, irreversible, stepwise losses of each component in proportion to its partial pressure at a given temperature. The first step of the simulation is to assess the initial molar ratios in the liquid phase. As described above, one can simply substitute fractional peak areas for fractional molar ratios without the need to calibrate for relative sensitivity factors of each compound. The equilibrium partial pressures were derived from the combination of Raoult's law, Dalton's law and Antoine constants for each compound in the mixture, as described previously [18, 26]. Raoult's law dictates that the partial vapor pressure p_A of A is proportional to the product of the mole fraction χ_A and the vapor pressure of the pure liquid p_A^*:

$$p_A = x_A p_A^*$$ Eq. 17

This law makes a fundamental assumption that the intermolecular interactions between unlike compounds are equal to the interactions between like compounds. The assumption is never strictly true but given the relative similarity of the intermolecular forces of all the hydrocarbons in this mixture, the assumption is reasonably valid. Dalton's law applies similar logic to the vapor phase and asserts that partial pressures are additive. The partial pressures at different temperatures were calculated from tabulated Antoine constants of Antoine plots, which are a semi-empirical form of the Clausius-Clapeyron equation that relates a substance's vapor pressure to the temperature.

Once the equilibrium partial pressures were calculated for the original, unweathered artificial gasoline, a total of 5% of the mixture was then subtracted to represent an irreversible evaporative loss, as would be expected from the weathering of volatile components. The 5% loss was distributed unevenly among the nine compounds in direct proportion to each components' partial pressure. Therefore, the most volatile components experienced the largest proportional losses and the least volatile components experienced the smallest proportional losses.

After the simulated stepwise loss, the remaining molar ratio of each component changes, so the new partial pressures must be recalculated. The fractional losses and equilibrium partial pressures were calculated in an iterative process until the mixture was weathered to the desired extent. Because each step represented a 5% evaporative loss, the fraction remaining after each iteration followed an exponential decrease as a function of the number of iterations. Step sizes of 2%, 1% and 0.5% per step provided higher resolution data, but did not provide meaningfully different results. However, step sizes larger than 5% per step provided significantly different and unrealistic proportional losses. The mathematical simulations of the artificial gasoline were completed using Microsoft Excel version 15 (Microsoft Corporation, Redmond, WA, USA).

The model supports the experimental observations in that the composition of weathered residues as a function of time—or extent of weathering—is significantly different at different temperatures. For example, in Figure 7, toluene falls below the limits of detection at 90% weathering and 30 °C but is still readily observable at ~1% of the total ion chromatogram (TIC) at 98% weathering and 210 °C. Such behavior could help explain why ignitable liquids that are highly weathered at elevated temperatures in structure fires are likely to resemble those weathered in the laboratory to a lesser extent at room temperature. Given a chromatogram of a pristine ignitable liquid, the model based on Raoult's law predicts the peak area of each weathered compound with a root mean squared error of prediction (RMSEP) of ~3% when the liquid is weathered up to 210 °C and 98%.

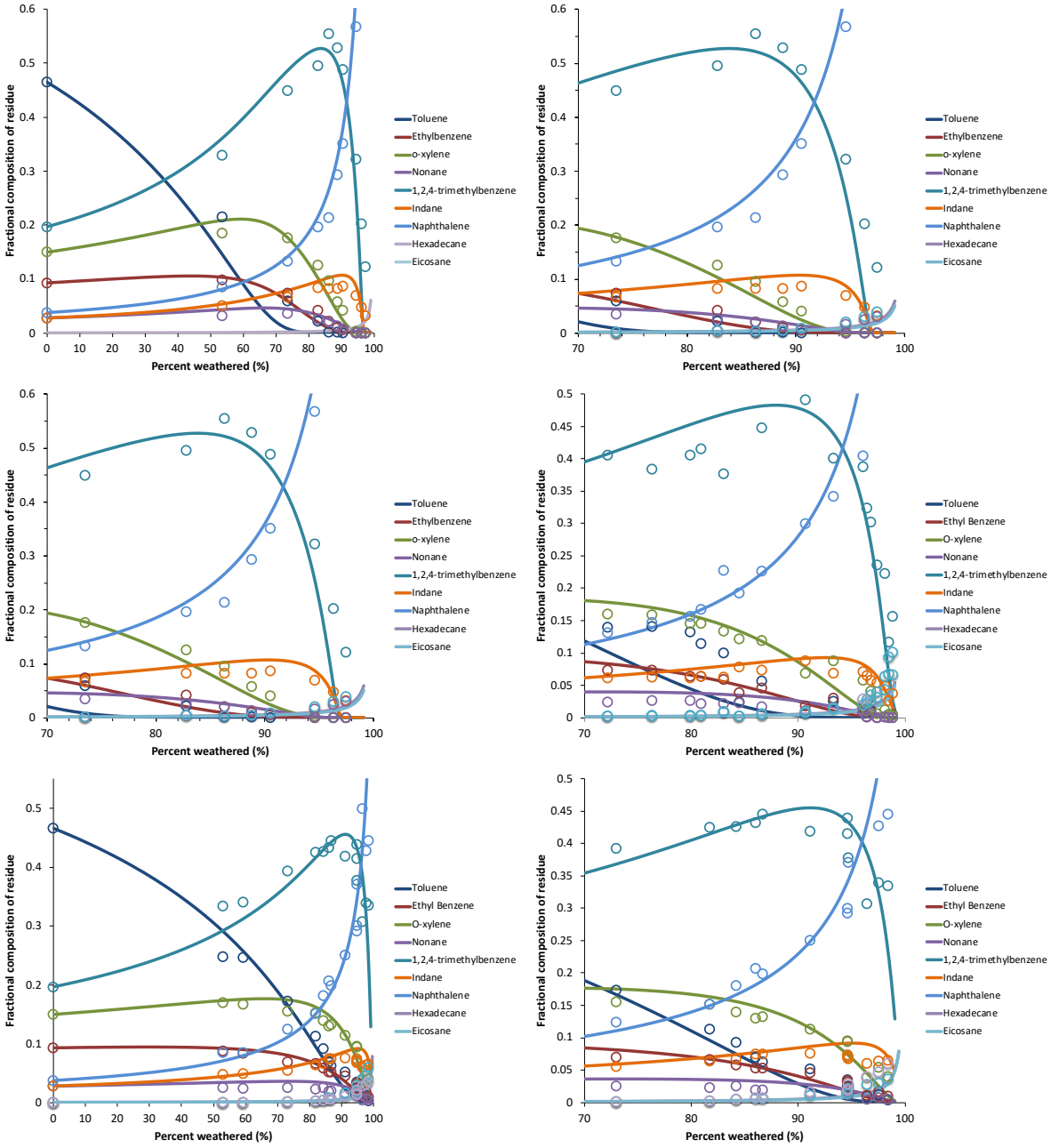

Figure 7. Overlay of experimentally collected weathering data (circles) and the mathematically modeled predictions (lines) for the artificial gasoline mixture for a) 30 °C, b) 30 °C expanded, c) 150 °C, d) 150 °C expanded, e) 210 °C, and f) 210 °C expanded.

This resource was prepared by the author(s) using Federal funds provided by the U.S. Department of Justice. Opinions or points of view expressed are those of the author(s) and do not necessarily reflect the official position or policies of the U.S. Department of Justice.

2.3 Activities and Accomplishments

Peer-reviewed publications

Willis IC, Fan Z, Davidson JT, Jackson GP. Weathering of Ignitable Liquids at Elevated Temperatures: A Thermodynamic Model, Based on Laws of Ideal Solutions, to Predict Weathering in Structure Fires. *Forensic Chem*istry 18, **2020**, 100215. https://doi.org/10.1016/j.forc.2020.100215.

*Conference presentations (presenting author underlined, † indicates graduate student, †† indicates undergraduate student, * indicates invited presentation)*

††Isaac C. Willis, Zilin Fan, †J. Tyler Davidson, Glen P. Jackson. The Influence of Elevated Temperatures on the Weathering of Ignitable Liquids. Poster presentation at the Pittsburgh Conference on Analytical Chemistry and Applied Spectroscopy, Philadelphia, PA, March 2019. (NIJ Poster session)

†Caitlyn Wensel, ††Isaac Willis, Zilin Fan, †J. Tyler Davidson, and Glen P. Jackson. The Effects of Elevated Temperatures and Substrates on the Weathering of Ignitable Liquids. Oral presentation at the 72nd American Academy of Forensic Sciences Annual Meeting, Anaheim, CA. February 2020.

†Caitlyn Wensel, ††Isaac C. Willis, Zilin Fan, †J. Tyler Davidson, †Natasha K. Eklund, †Amanda L. Setser, Victoria L. McGuffin, Ruth Waddell Smith, and Glen P. Jackson. Thermodynamic and Kinetic Predictions of the Evaporation Patterns of Ignitable Liquids at Elevated Temperatures. Oral presentation at the 71st Annual Pittsburgh Conference on Analytical Chemistry and Applied Spectroscopy (Pittcon), Chicago, IL. March 2020.

††Hannah L. McMillen, Glen P. Jackson. Evaluation of a Thermodynamic Model to Predict the Weathering of Ignitable liquids at Elevated Temperatures. Oral presentation at the 74th American Academy of Forensic Sciences Annual Meeting, Seattle, WA. February 2022.

††Ahna Kotula, Glen P. Jackson. The Weathering of Ignitable liquids at Elevated Temperatures. Poster presentation at the Chesapeake Bay Division of the International Association for Identification (CBD-IAI), Gettysburg, PA. March 2022.

2.4 Limitations and Areas of Future Work

Our modeling above shows that, whereas the extent of weathering is still a significant factor when considering the relative distribution of residues in weathered ignitable liquids, the role of temperature cannot be ignored. When the extent of evaporation is kept constant, weathering at higher temperatures leaves greater quantities of volatile components in the residue. When the composition of a liquid is known, the composition of each component in the residue can be predicted with a root mean squared error prediction of around 3%, even up to 98% weathering.

The major limitation of this approach is that the identity of each component is necessary to predict the vapor pressure of each component. One of the goals of the next phase of the model, and to make the model more practical for complex mixtures of unknown substances, was to enable the model to accurately predict vapor pressures and evaporation behaviors without needing to know the identity of every compound in the chromatogram. Such calculations are possible because of the strong correlation between boiling point, vapor pressure and retention index, as shown above in Figures 2 and 4.

There are at least two ways in which one could make practical use of the ability to model the evaporation of complex liquids. First, the model could be applied to databases of pristine ignitable liquids to provide laboratories with huge in-house databases of weathered samples. This capability would circumvent their need to perform any experimental weathering of ignitable liquids and thereby save time, money, environmental impact, resources, and chemical waste. Second, this model might be able to distinguish between liquids that have been weathered at room temperature, in the absence of fire, versus liquids that have been weathered at elevated temperatures. To enable this benefit, one would also need to assess the effects of temperature variations during the simulated weathering. Such modifications to the model are relatively straightforward, but the variety of temperatures and times that require modeling might require impractical computational power.

Goal 3: Investigate the kinetic and thermodynamic approaches for accurate prediction of gasoline evaporation at temperatures up to 210 °C.

Comparison of the kinetic and thermodynamic models not initially possible as each model is based on a different foundation, produces a different output, and the models have been validated using different samples and metrics. To enable a comprehensive evaluation of the models, it was necessary to first address and overcome these inconsistencies by deriving kinetic and thermodynamic models that were based on the same foundational theory. A common data set of normal alkanes was used to generate a kinetic model based on evaporation rate constants and a thermodynamic model based on standard vapor pressures. The performance of the models was then evaluated in two ways. First, the error in predicting abundance of individual compounds in evaporated gasoline samples was determined and second, the correlation between the predicted and experimental chromatograms of the evaporated gasoline samples was determined.

3.1 Research Design and Methods

3.1.1 Deriving kinetic and thermodynamic models to predict evaporation on the same foundational basis

The kinetic model developed by McIlroy *et al.* is an irreversible kinetic model in which the system is assumed to be fully open, with substance *X* transferred from the liquid phase (*L*) to the gas phase (*G*)

$$X_L \xrightarrow{k} X_G \qquad \text{Eq. 18}$$

where *k* is the evaporation rate constant. The rate of change in concentration of X_L as a function of time, *t*, is given by the rate law

$$\frac{-d[X_L]}{dt} = k[X_L] \qquad \text{Eq. 19}$$

and, on separating variables and integrating, the integrated rate law describing evaporation in an irreversible system is given by

$$\frac{[X_L]}{[X_L]_0} = exp(k\,t) \qquad \text{Eq. 20}$$

In a reversible kinetic model, the system is assumed to be closed, such that substance *X* is transferred between the liquid and gas phases

$$X_L \underset{k'}{\overset{k}{\rightleftharpoons}} X_G \qquad \text{Eq. 21}$$

where *k'* is the rate constant for condensation. In this case, the rate law is given by

$$\frac{-d[X_L]}{dt} = k[X_L] - k'[X_G] \qquad \text{Eq. 22}$$

If the initial concentration of molecule *X* in the gas phase is zero ($[X_G]_0$), then the concentration of *X* in the gas phase at any time can be expressed in terms of the concentration in the liquid phase

$$[X_G] = ([X_L]_0 - [X_L])(V_L/V_G) \qquad \text{Eq. 23}$$

where V_L and V_G are the volumes of the liquid and gas phases, respectively. By substituting Eq. 23 into Eq. 22, the rate law for the reversible system is given by

$$\frac{-d[X_L]}{dt} = k[X_L] - k'([X_L]_0 - [X_L])(V_L/V_G) \qquad \text{Eq. 24}$$

On separating the variables and integrating, the integrated rate law describing evaporation in a reversible system is given by

$$\frac{([X_L]-[X_L]_{EQ})}{[X_L]_0-[X_L]_{EQ}} = exp\left(-\left(k + k'\left(\frac{V_L}{V_G}\right)\right) t\right) \qquad \text{Eq. 25}$$

where $[X_L]_{EQ}$ is the concentration of *X* in the liquid phase at equilibrium, which can be expressed in terms of the rate constants for evaporation and condensation (k and k', respectively) or by the equilibrium constants ($K_{EQ} = k/k'$) for evaporation, which are equal to the standard vapor pressures.

$$[X_L]_{EQ} = \frac{k'(V_L/V_G)}{k+ k'(V_L/V_G)}[X_L]_0 = \frac{1}{1+K_{EQ}(V_G/V_L)}[X_L]_0 \qquad \text{Eq. 26}$$

3.1.2 Retention index as a surrogate for rate constant and standard vapor pressure

From the theoretical approach described in Section 3.1.1, Eq. 20 and Eq. 26 represent kinetic and thermodynamic models of evaporation, respectively, that are derived from the same foundational basis. However, at this stage, both approaches require that compounds be identified or otherwise known so that the relevant properties (rate constants and equilibrium constants for evaporation) can be determined. To overcome this limitation, retention index was used as a surrogate for evaporation rate constant in the kinetic approach and for standard vapor pressure in the thermodynamic approach.

The natural logarithm of the experimentally determined evaporation rate constants at 20 °C for *n*-alkanes ranging from C_8 – C_{13} [19] were plotted as a function of I^T and linear regression was used to define the relationship

$$ln\, k = -1.20 \times 10^{-2} I^T + 8.098 \qquad \text{Eq. 27}$$

In a similar manner, standard vapor pressures at 20 °C for each *n*-alkane were calculated using the Antoine equation with coefficients from the NIST Chemistry Webbook [27, 28]. The natural logarithm of the standard vapor pressure, $ln\, P^0$, was plotted as a function of I^T and linear regression was used to define the relationship

$$ln\, K_{EQ} = ln\, P^0 = -1.25 \times 10^{-2} I^T + 5.722 \qquad \text{Eq. 28}$$

The coefficient of determination (R^2) indicated a high-quality fit for both regression analyses (R^2 = 0.9969 and 0.9998 for the kinetic and thermodynamic approaches, respectively). As such, Eqs. 27 and 28 now provide a means to predict an evaporation rate constant (k) or a standard vapor pressure (P^0) as a function of retention index.

3.1.2.1 Retention index as a surrogate for vapor pressure in the iterative thermodynamic model
Following the same strategy as above—which is to eliminate the need to identify compounds to predict their evaporation rates or vapor pressures—we also used retention indices to predict vapor pressures for the iterative thermodynamic model. We used the same relationships described above, and Antoine constants from Yaws and NIST [25, 27].

The plots shown in Figure 8 enable the prediction of vapor pressures of unknown substances in complex mixtures. For the thermodynamic model, these vapor pressures can then be used to estimate the extent of weathering of each substance in a chromatogram, just as the model had done before for the 9-component mixture.[3,4] The results are described in section 3.2.2.

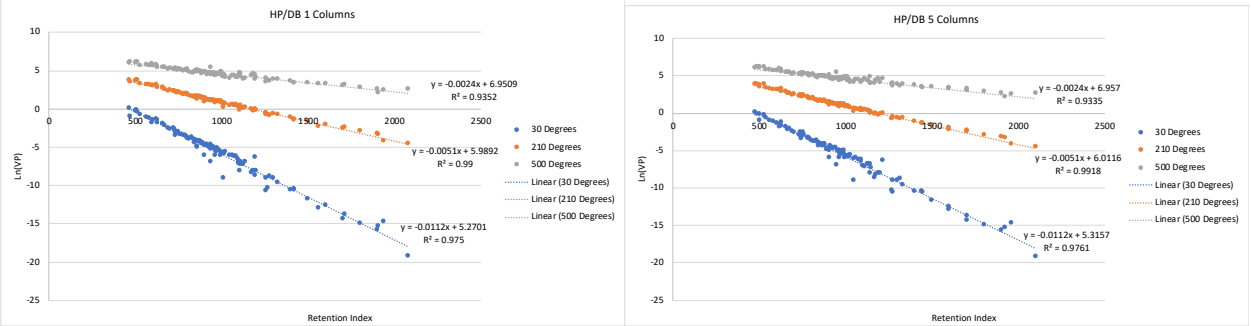

Figure 8. Plots to show the relationships between ln(vapor pressure) versus retention index for two of the most common types of GC stationary phases.

3.1.3 Predicting evaporation using the kinetic and thermodynamic approaches

In general, to predict chromatograms corresponding to evaporated liquids, the fraction remaining of a given compound at a given I^T is determined using Eq. 4 as described in Goal 1. For the kinetic approach here, the evaporation rate constant can be predicted from Eq. 27 and substituted into the kinetic model defined in Eq. 20

$$F_{I^T} = \frac{[X_L]}{[X_L]_0} = exp(k\ t) = exp(-exp(-1.20\ \times 10^{-2} I^T + 8.098)\ t) \qquad \text{Eq. 29}$$

Similarly, the standard vapor pressure can be predicted from Eq. 28 and substituted into the thermodynamic model defined in Eq. 26

$$F_{I^T} = \frac{[X_L]}{[X_L]_0} = \frac{1}{1+K_{EQ}(V_G/V_L)} = \frac{1}{1+exp(-1.25 \times 10^{-2} I^T + 5.722)(V_G/V_L)} \qquad \text{Eq. 30}$$

Thus, the fraction remaining of a compound at a given I^T (F_{I^T}) is determined using Eq. 29 for the kinetic approach and using Eq. 30 for the thermodynamic approach. The total fraction remaining (F_{Total}) is then calculated using Eq. 7. As described in Goal 1, the models can be used to predict chromatograms corresponding to the same F_{Total} value represented by the experimental chromatogram. In the kinetic approach, t in Eq. 29 is varied to reach the required F_{Total} whereas, in the thermodynamic approach, V_G/V_L is varied in Eq. 30.

This resource was prepared by the author(s) using Federal funds provided by the U.S. Department of Justice. Opinions or points of view expressed are those of the author(s) and do not necessarily reflect the official position or policies of the U.S. Department of Justice.

3.1.4 Evaluating the kinetic and thermodynamic approaches to predict evaporation of gasoline

3.1.4.1 Sample preparation

Regular, unleaded gasoline was collected from a local service station and stored at 4 °C until analysis. A 10-µL aliquot of gasoline was transferred to a 2-mL volumetric flask, 20 µL of *n*-tetradecane (C_{13}, 0.051 M) was added, and the samples were diluted to volume with CH_2Cl_2. Additional aliquots of undiluted gasoline were evaporated to nominal F_{Total} levels of 0.7, 0.5, 0.3, and 0.1 by volume, which correspond to evaporation levels of 30, 50, 70, and 90%. Evaporations were conducted in triplicate in a 10-mL measuring cylinder, with agitation and under a flow of nitrogen. Once evaporated to the required level, CH_2Cl_2 was added to bring the total volume back up to 10 mL and a 10-µL aliquot of the diluted sample was transferred to a 2-mL volumetric flask. A 20-µL aliquot of C_{13} (0.051 M) was added as an internal standard and the solution was diluted to volume with methylene chloride. A retention index ladder was also prepared by diluting reference standards of *n*-alkanes from *n*-pentane to *n*-tetradecane (C_5 – C_{14}, 0.0072 – 0.0032 M) in CH_2Cl_2.

3.1.4.2 GC-MS analysis

Unevaporated gasoline, evaporated gasoline, and the retention index ladder were all analyzed by GC-MS, using the same instrument as described in Section 1.1.4. Instrument parameters were consistent with those previously described with the exception of the oven temperature program and the time during which the detector was turned off. For these analyses, the oven temperature program was based on that used by the National Center for Forensic Science [6]: initial oven temperature 40 °C for 3 min, followed by a 10 °C/min ramp to 280 °C, with a final hold time of 4 min and a transfer line temperature of 280 °C. In addition, the detector was turned off from 1.65 – 1.88 min during elution of the CH_2Cl_2 solvent. All other parameters were consistent with those described in Section 1.1.4.

3.1.4.3 Data analysis

Total ion chromatograms of the unevaporated and evaporated gasoline samples and the retention index ladder were exported from the ChemStation software into Microsoft Excel for subsequent processing. Retention indices were calculated using Eq. 8 (following the procedure described in Section 1.1.5) and each experimental chromatogram was then normalized to the peak abundance of the C_{13} internal standard. The F_{Total} by area was calculated for each evaporated gasoline by dividing the area under the chromatogram by the area under the chromatogram of the unevaporated gasoline.

The kinetic and thermodynamic models (Eq. 29 and 30, respectively) were then used to predict chromatograms corresponding to the F_{Total} levels calculated for the experimental chromatograms. For the kinetic model, t in Eq. 29 was varied to reach the desired F_{Total} level while for the thermodynamic model, V_G/V_L in Eq. 30 was varied. To generate the predicted chromatogram, the fraction remaining at each retention index was multiplied by the normalized abundance in the unevaporated gasoline at the corresponding retention index.

The performance of the kinetic and thermodynamic approaches was evaluated based on the error and mean absolute percent error (Eq. 9 and 10, respectively) in predicting abundance of selected compounds and based on the correlation between the predicted and experimental chromatograms (Eq. 11).

3.2 Results and Findings

3.2.1 Error in predicting abundance of representative gasoline compounds

Representative chromatograms of experimentally evaporated gasoline corresponding to F_{Total} levels of 0.7, 0.5, 0.3, and 0.1 are shown in Fig. 9, along with corresponding chromatograms predicted using the kinetic and the thermodynamic approaches.

Overall, there was a high degree of similarity among the chromatograms predicted by each model (Fig. 9B and C) and the corresponding experimental chromatograms of evaporated gasoline (Fig. 9A). At higher F_{Total} levels (F_{Total} = 0.7 and 0.5), the abundances of the more volatile compounds (I^T < 800) were very similar between the two models. However, as evaporation level increased (F_{Total} = 0.3), some minor differences were observed between the predicted chromatograms. Using the kinetic model (Fig. 9B), compounds with I^T < 650 were predicted to be completely evaporated, with very low abundance of compounds in the range 650 < I^T < 700. In contrast, the thermodynamic model (Fig. 9C) predicted a measurable abundance of all compounds with I^T < 700 at F_{Total} = 0.3. At the highest evaporation level (F_{Total} = 0.1), the kinetic model (Fig. 9B) predicted complete evaporation of all compounds with I^T < 945 while the thermodynamic model (Fig. 9C) predicted measurable abundance of compounds in this range. Both models predicted similar abundances at each F_{Total} level for less volatile compounds that elute with I^T > 1000.

The error in predicted abundance of several alkylbenzenes representative of gasoline was also calculated for both approaches to provide a quantitative metric for evaluation (Table 5). At F_{Total} = 0.7, the percent errors in predicting abundance of the alkylbenzenes were very similar for the two models, with both yielding a mean absolute percent error in prediction of 2.0%. As F_{Total} level decreased, prediction errors increased for both models. At F_{Total} = 0.5 and 0.3, the mean absolute percent error in prediction was 4.4% and 8.7% for the kinetic model, respectively, and 5.3% and 12.1% for the thermodynamic model, respectively. The greatest difference in predictive accuracy between the two models occurred at F_{Total} = 0.1, which corresponded to an evaporation level of 90%. At this level, the alkylbenzenes had undergone significant evaporation, which resulted in a large % error in predicting abundance of individual compounds (*e.g.*, -70.5% and 911% error using the kinetic and thermodynamic models, respectively, to predict the abundance of ethylbenzene, I^T = 844, Table 5). As such, the mean absolute percent errors were large (54.9% and 279% for the kinetic and thermodynamic models, respectively) although do demonstrate improved accuracy in the kinetic model at the lower F_{Total} levels.

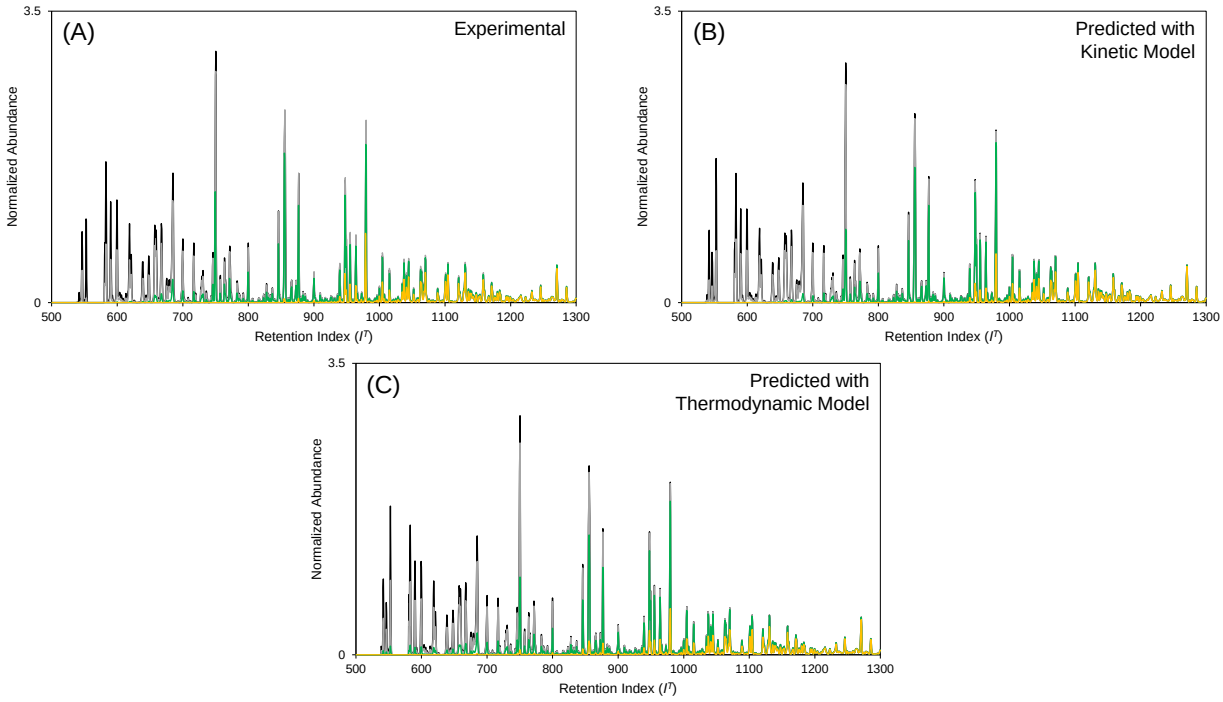

Figure 9. Predicting evaporation of gasoline (A) experimental chromatograms of evaporated gasoline, (B) chromatograms predicted using the kinetic model, and (C) chromatograms predicted using the thermodynamic model. In each plot, chromatograms are colored according to F_{Total} level as follows: F_{Total} = 0.7 in black, F_{Total} = 0.5 in grey, F_{Total} = 0.3 in green, and F_{Total} = 0.1 in yellow.

Table 5. Percent error and mean absolute percent error in predicting abundance of alkylbenzenes in evaporated gasoline using the kinetic and thermodynamic approaches

Alkylbenzene	Retention Index	Error (%)[a] in Kinetic Model at each F_{Total}				Error (%) in Thermodynamic Model at each F_{Total}			
		0.7[b]	0.5	0.3	0.1	0.7	0.5	0.3	0.1
Toluene	750	-4.6	-5.7	-33.8	-100	-4.9	-8.4	-29.7	$7.6x10^4$
Ethylbenzene	844	-1.5	-3.5	5.5	-70.5	-1.5	-4.4	-6.8	911
p-Xylene	853	-1.8	-4.3	-9.5	-81.6	-1.8	-5.2	-19.8	254
o-Xylene	876	-2.4	-4.6	0.05	-59.8	-2.4	-5.2	-10.1	183
Ethylmethylbenzene	945	0.4	-2.4	2.4	-33.0	0.4	-2.6	-3.3	-15.9
1,2,4-trimethylbenzene	978	-1.2	-6.0	1.1	-29.5	-1.2	-6.1	-3.0	-33.2
Mean absolute percent error[c]		**2.0**	**4.4**	**8.7**	**54.9[d]**	**2.0**	**5.3**	**12.1**	**279[d]**

a Percent error calculated using Eq. 9
b Nominal F_{Total} value shown but all calculations and prediction used the exact F_{Total} by area
c Mean absolute percent error calculated using Eq. 10
d Mean absolute percent error calculated using Eq. 10, omitting toluene from the calculation

Correlation between the predicted and experimental chromatograms was also evaluated using PPMC coefficients to evaluate the extent of similarity (Table 6). At each F_{Total} level, PPMC coefficients demonstrated comparable correlation using each model. While coefficients decreased as F_{Total} level decreased, strong correlation between predicted and experimental chromatograms was maintained for

This resource was prepared by the author(s) using Federal funds provided by the U.S. Department of Justice. Opinions or points of view expressed are those of the author(s) and do not necessarily reflect the official position or policies of the U.S. Department of Justice.

both models. Overall, despite some differences in performance, both models were demonstrated to work well to predict evaporation of gasoline at 20 °C.

Table 6. PPMC coefficients for comparison of experimental chromatograms of evaporated gasoline to corresponding chromatograms predicted using the kinetic and thermodynamic approaches

Nominal F_{Total}	F_{Total} by Area[a]	PPMC Coefficients[b]	
		Kinetic Model	Thermodynamic Model
0.7	0.9257	0.9913	0.9903
0.5	0.8270	0.9901	0.9853
0.3	0.5392	0.9426	0.9420
0.1	0.1974	0.9068	0.8921

a F_{Total} by area calculated as area under chromatogram of evaporated liquid divided by area under chromatogram of corresponding unevaporated liquid
b PPMC coefficients calculated using Eq. 11

3.2.2 Extension and initial validation of kinetic and thermodynamic models

The unified kinetic and thermodynamic approach described in section 3.2.1 was developed based only on the rate constants and vapor pressures of *n*-alkanes at 20 °C. To continue this approach, the next step is to include additional compound classes in model development and to develop variable-temperature models.

To that end, an additional 20 compounds spanning two compound classes (alkyl benzenes and cycloalkanes) were included in model development. These compounds were selected as experimentally determined rate constants at five temperatures (5, 10, 20, 30, and 35 °C) and Antoine coefficients to calculate vapor pressures at the corresponding temperatures were readily available. For the kinetic models, the natural logarithm of rate constant at each temperature was plotted as a function of I^T and linear regression was performed to define each fixed-temperature model. Using the same data, multiple linear regression was performed to define the variable-temperature model. The thermodynamic models were developed in a similar manner albeit using calculated vapor pressures at each temperature rather than rate constants. The regression coefficients for the three-class models are summarized in Table 7 for the kinetic models and in Table 8 for the thermodynamic models.

Table 7. Fixed- and variable-temperature kinetic models developed based on evaporation rate constants for 26 compounds representing three compound classes (*n*-alkanes, alkyl benzenes, and cycloalkanes).

Temperature (°C)	Slope (m_1)	Slope (m_2)	Intercept (b)	Coefficient of Determination (R^2)
5	-1.22×10^{-2}	-	7.80	0.9918
10	-1.19×10^{-2}	-	7.59	0.9841
20	-1.12×10^{-2}	-	7.54	0.9934
30	-1.09×10^{-2}	-	8.12	0.9967
35	-1.09×10^{-2}	-	8.68	0.9915
Variable	-1.12×10^{-2}	-6030	28.4	0.9821

General form for fixed-temperature models: $\ln(k) = m_1 I^T + b$
General form for variable-temperature model: $\ln(k) = m_1 I^T + m_2 (1/T) + b$

Table 8. Fixed- and variable-temperature thermodynamic models developed based on calculated Antoine coefficients for 26 compounds representing three compound classes (*n*-alkanes, alkyl benzenes, and cycloalkanes).

Temperature (°C)	Slope (m_1)	Slope (m_2)	Intercept (b)	Coefficient of Determination (R^2)
5	-1.33×10^{-2}	-	5.73	0.9875
10	-1.28×10^{-2}	-	5.68	0.9885
20	-1.20×10^{-2}	-	5.59	0.9903
30	-1.13×10^{-2}	-	5.52	0.9919
35	-1.09×10^{-2}	-	5.50	0.9926
Variable	-1.21×10^{-2}	-5934	25.9	0.9868

General form for fixed-temperature models: $\ln(P^0) = m_1 I^T + b$
General form for variable-temperature model: $\ln(P^0) = m_1 I^T + m_2 (1/T) + b$

The fixed- and variable-temperature models for both approaches are currently being evaluated. So far, the models have been used to predict evaporation rate constants and vapor pressures for each compound included in model development (Appendix 1, Tables A1.1 – A1.4). For the fixed- and variable-temperature kinetic models, the overall mean absolute percent error in prediction was 11.4% and 19.0%, respectively. Performance of the thermodynamic models was comparable, with an overall mean absolute percent error in prediction of 15.2% and 19.0% for the fixed- and variable-temperature models, respectively. As we continue this validation, errors in predicting chromatograms corresponding to evaporated liquids will also be evaluated.

3.2.3 Results of iterative thermodynamic model to model the evaporation of gasoline

We have now completed experimental weathering of a real gasoline sample at a variety of extents of evaporation at 30, 90, and 120 °C using a vessel of 'ideal' geometry. The procedure involves the evaporation of 1 mL aliquots of gasoline in a shallow aluminum weigh boat and therefore provides a large surface area-to-volume ratio, which our past work had shown to works reliably for a simulated gasoline mixture [18, 24]. Some of the results of the new gasoline weathering at 30 °C are shown in **Figure 10**. **Figure 11** shows the experimental data points for the fractional composition of three major compounds of interest in E85 gasoline; toluene, 1,2,4-trimethylbenzene and naphthalene, are plotted relative to the simulations.

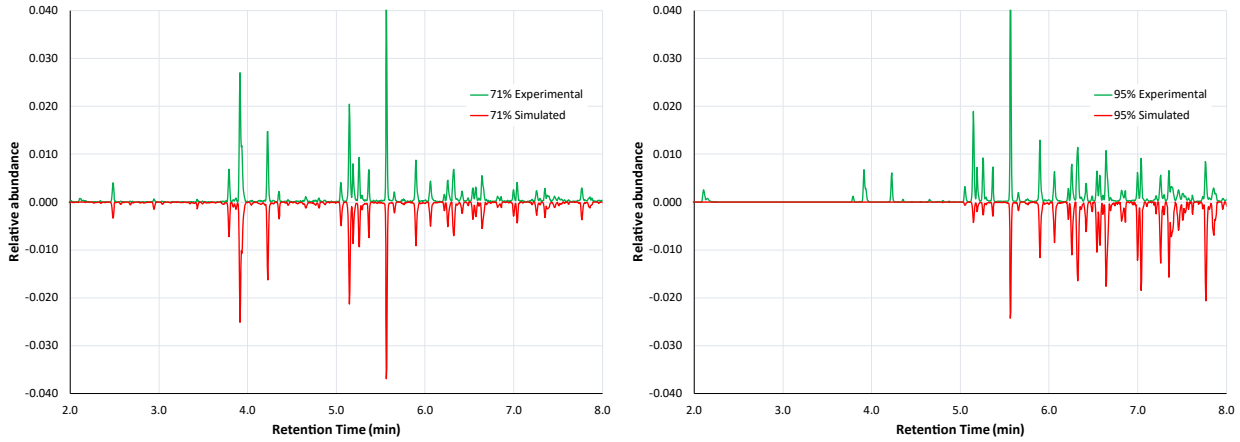

Figure 10. Plots to show the predicted fractional abundance relative to gasoline weathered to (A) 71% and (B) 95%.

We have also conducted correlation analyses (PPMC coefficients) between each simulated chromatogram and each weathered chromatogram to see which simulated extent of weathering best matched each experimental condition. The closest correlation between the model and the 71% weathered experimental data was for gasoline simulated at 71% weathering. Although the model was accurate for this particular sample, the model was typically less accurate across the other 20 weathered samples. For example, for one of the gasoline samples weathered to 95%, the PPMC coefficient for the simulated weathering maximized at 0.991 at 86% weathering, which is a 9% error in the percent weathering. Using the maximum PPMC coefficient as an estimate of percent weathering for the 21 weathered samples from 21-95% weathering, the mean absolute error in predicting the extent of weathering was ~6%.

For samples weathered more than 70%, the model consistently underestimates the extent of weathering by 6-10% (Figure 10B), which indicates that the experimental samples contain slightly greater abundances of volatiles than the model would predict. The model holds true at elevated temperatures, too, and we have identified the problem to be that the modeling is unable to account for the evaporative losses of volatile components that elute before the solvent delay. We are therefore incorporating a correction term into the model to account for the evaporative losses of volatiles for which no chromatographic data exists. Such a correction term is only possible at the level of ignitable liquid class because in the application to true unknowns, it will not be possible to know what proportion of the ignitable liquid (or it's residue) elutes before the solvent delay.

This resource was prepared by the author(s) using Federal funds provided by the U.S. Department of Justice. Opinions or points of view expressed are those of the author(s) and do not necessarily reflect the official position or policies of the U.S. Department of Justice.

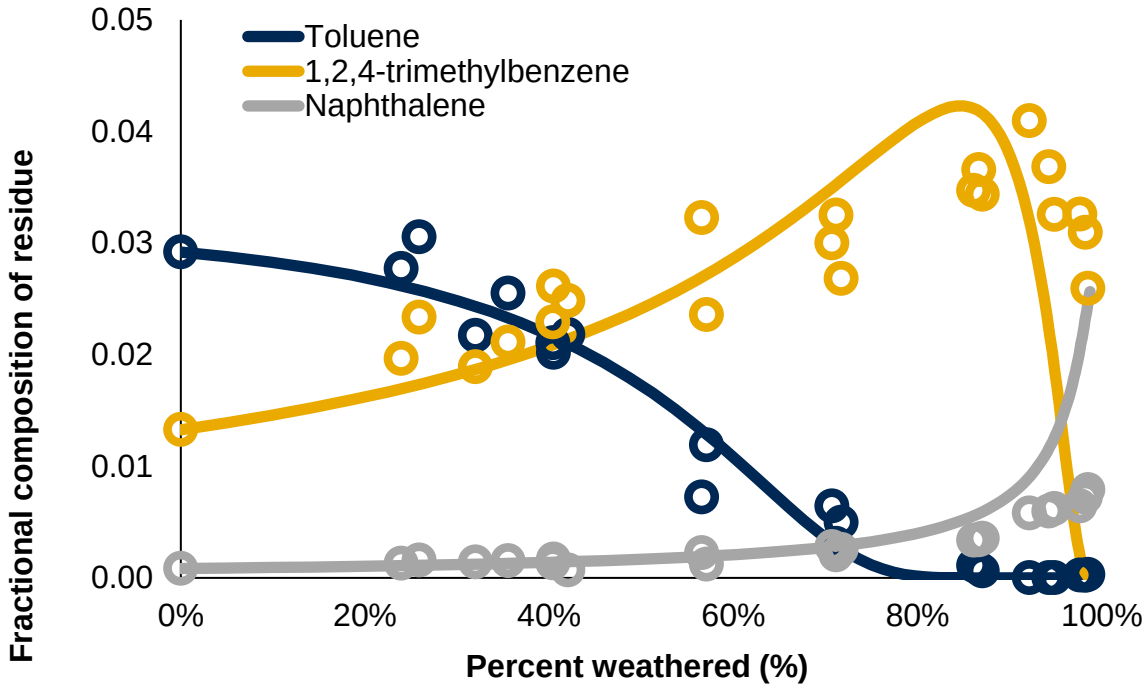

Figure 11. Overlay of experimentally collected weathering data (circles) and the mathematically modeled predictions (solid lines) for E85 gasoline residues of toluene (blue), 1,2,4-trimethylbenzene (gold) and naphthalene (gray) at 30 °C.

3.3 Activities and Accomplishments

Peer-reviewed publications

McGuffin VL, Waddell Smith R. A Unified Kinetic and Thermodynamic Model of Evaporation for Forensic Applications. *Forensic Chemistry* **2021**, *23*, 100304. https://doi.org/10.1016/j.forc.2020.100304.

*Conference presentations (presenting author underlined, † indicates graduate student, †† indicates undergraduate student, * indicates invited presentation)*

Victoria L. McGuffin and Ruth Waddell Smith. Kinetic and Thermodynamic Models of Evaporation for Forensic Applications. Oral presentation at the SciX Conference, Palm Springs, CA. October 2019.

††Hannah L. McMillen, Glen P. Jackson. Evaluation of a Thermodynamic Model to Predict the Weathering of Ignitable liquids at Elevated Temperatures. Oral presentation at the 74th American Academy of Forensic Sciences Annual Meeting, Seattle, WA. February 2022.

††Ahna Kotula, Glen P. Jackson. The Weathering of Ignitable liquids at Elevated Temperatures. Poster presentation at the Chesapeake Bay Division of the International Association for Identification (CBD-IAI), Gettysburg, PA. March 2022.

3.4 Limitations and Areas of Future Work

In this goal, a unified kinetic and thermodynamic approach to model evaporation was developed and the predictive accuracy of both approaches was demonstrated. Models were developed using only *n*-alkanes and using selected compounds representative of three compound classes (*n*-alkanes, alkylbenzenes, and cycloalkanes). Future work will focus on full evaluation of the three-class models and development of additional models that include more compound classes. We are currently considering branched alkanes and polycyclic aromatic hydrocarbons as the additional compound classes. Evaporation rate constants and calculated vapor pressures for the additional branched alkanes and polycyclic aromatic hydrocarbons will be included with our current data sets to develop fixed- and variable-temperature models. The accuracy of each model in predicting evaporation of gasoline at different temperatures will be evaluated based on correlation between predicted and experimental chromatograms and based on abundance of selected compounds.

For the iterative thermodynamic model, the extra correction term to account for unobservable volatiles in the chromatograms is still being tested. For the gasoline sample in question, which contained approximately 15% by volume of ethanol among other volatiles eluting in the solvent delay, we are finding that the models are more accurate when we add approximately 18% to the total peak area and allow this portion of the liquid to have an average volatility equal to that of ethanol. PPMC values and MARs are now maximizing and minimizing, respectively, at modeled extents of weathering that are typically within 5% of the experimental values.

Goal 4: Demonstrate the application of the kinetic and thermodynamic approaches to identify gasoline at any evaporation level in fire debris samples.

Chromatograms of fire debris samples submitted to a laboratory for analysis are typically compared to a reference collection of known liquids evaporated to different levels to identify any liquid present. Due to the likely presence of substrate interferences in chromatograms of fire debris samples, analysts often compare not just the total ion chromatogram (TIC) but also, extracted ion profiles (EIPs) corresponding to different compound classes. However, given the time- and resource-intensive nature involved in evaporating reference liquids, not every liquid in a laboratory reference collection will be evaporated and may only be evaporated to a limited number of levels.

The kinetic model can be used to identify liquids present in fire debris samples. For this application, the model is used to predict chromatograms corresponding to different F_{Total} levels for any liquid in the reference collection. Further, extracted ion profiles corresponding to specific compound classes can be predicted in a similar manner. As such, a reference collection of predicted TICs and EIPs can be generated in a timely manner. The TIC and relevant EIPs from a submitted fire debris sample can then be compared to the predicted reference collection to identify the liquid present based on strongest correlation between the submitted sample and the predicted reference collection.

In Goal 4, the focus was to demonstrate the application of the kinetic model to be used as a tool in forensic laboratories to identify ignitable liquids in fire debris samples. The first step was to demonstrate wider application of the model to predict evaporation of liquids from different classes identified by ASTM International [4]. Then, the model was applied to predict EIPs corresponding to relevant compound classes for each liquid. Once the accuracy in predicting TICs and EIPs was demonstrated, the model was used to generate predicted TIC and EIP reference collections. Chromatograms of fire debris

samples collected from large-scale burns were then compared to the reference collections to identify the ignitable liquid present.

4.1 Research Design and Methods

4.1.1. Ignitable liquid evaporation

Fifteen ignitable liquids representing five classes (isoparaffinic, naphthenic-paraffinic, aromatic, petroleum distillate, and gasoline) were experimentally evaporated to three levels: 50%, 70%, and 90% (corresponding to F_{Total} = 0.5, 0.3, and 0.1, respectively). To do this, 10 mL of the unevaporated liquid was placed in a measuring cylinder along with a stir bar. Using a flow of nitrogen, the liquids were evaporated to 5 mL, 3 mL and 1 mL with stirring. The evaporated liquid was diluted back to the 10-mL mark with CH_2Cl_2. Evaporated samples were diluted further (1:200 v/v) with CH_2Cl_2 and an appropriate internal standard was added (1:100 v/v) to the sample. For liquids with compounds eluting in the range I^T = 500 – 1350, *n*-tetradecane (C_{14}, 0.051 M) was added as the internal standard, whereas for liquids with compounds eluting in the range I^T = 1100 – 1650, *n*-heptadecane (C_{17}, 0.020 M) was added. The unevaporated equivalent of the 15 liquids, in addition to kerosene and diesel, was also prepared for analysis by diluting the unevaporated liquid (1:200 v/v) with CH_2Cl_2 and adding the appropriate internal standard.

In addition to the known liquids, five single-blind samples (Sample A – E) were prepared by other analysts in the laboratory. Samples A – C were selected from the set of 15 liquids while Samples D and E were new liquids that were not present in the set. The five single-blind samples were evaporated to different levels and prepared for analysis following the procedures described above. Throughout the analysis and prediction steps, the identity of the liquid and the F_{Total} level remained unknown to the analyst.

For retention index calculations, a mixture of gasoline and diesel (1:5 v/v) was prepared and diluted in CH_2Cl_2 (1:50 v/v). The mixture was analyzed each day that samples were analyzed and used to calculate retention indices for samples analyzed on that day, following the procedure described in Section 1.1.5. It is worth noting here that the gasoline:diesel mixture contains *n*-alkanes spanning the retention range of interest and therefore was used as a readily available alternative to a separately prepared alkane ladder.

4.1.2 Large-scale burns

Large-scale burns were conducted at the New England Fire Investigation Seminar at Saint Anselm College in Manchester, NH in spring 2019. Three large containers (2.4 m x 4.9 m x 2.5 m) were fitted with olefin carpet and furnished with various common items including couches, love seats, curtains, and coffee tables. Gasoline was poured throughout two containers and paint thinner was poured throughout the third container to act as accelerants. The containers were ignited with a blow torch and allowed to burn for approximately 10 min (past flashover) before being extinguished with water. Several debris samples were collected from each container, including samples from areas where liquid was poured and samples from locations where no liquid was poured. The debris samples were collected in unlined metal paint cans and transported back to the laboratory for further processing.

Ignitable liquid residues were extracted from each debris sample following the passive-headspace extraction method outlined in ASTM E1412 [5]. One third of an activated carbon strip was suspended in the headspace above the debris sample, the paint cans were sealed and then placed in an oven at 80 °C for 4 h. Following the extraction, the paint cans were removed from the oven and the carbon strips were

removed. Carbon strips were extracted with 300 µL CH_2Cl_2 which was collected in a GC vial and 50 µL of *n*-tetradecane (C_{14}, 0.0010 M) was added as an internal standard.

4.1.3 GC-MS analysis

The unevaporated liquids, evaporated liquids, single-blind samples, large-scale burn samples, and gasoline:diesel mixtures were analyzed in triplicate by GC-MS. The instrument and instrument parameters were the same as those described in Section 1.1.4 except for the oven temperature program. In this case, the temperature program was the same as that used by the National Center for Forensic Science (NCFS) to analyze samples for their reference collection [6]: 40 °C for 3 min, 10 °C/min to 280 °C, with a final hold for 4 min. For all samples, the detector was turned off between 1.56 and 1.80 min, during solvent elution while for the gasoline:diesel mixture, the detector was turned off between 1.58 and 1.80 min. The slightly shorter time range was used to allow *n*-pentane (C_5) to elute and, therefore, be included in the retention index ladder.

4.1.4 Data analysis

Major compounds in the TIC of each sample were identified based on mass spectral comparison to the NIST/EPA/NIH Mass Spectral Library using the probability-based matching algorithm in ChemStation. Extracted ion profiles corresponding to five major compound classes were also generated in ChemStation using the following *m/z* values: alkanes (*m/z* 57, 71, 85, 99); aromatic (*m/z* 91, 105, 119, 133); indane (*m/z* 117, 131, 145, 159); and polynuclear aromatic (*m/z* 128, 142, 156). The TICs and EIPs were then exported from ChemStation into Microsoft Excel for further processing.

Retention indices were calculated for the unevaporated, evaporated, single-blind, and large-scale burn samples following the procedure described in Section 1.1.5. The F_{Total} levels for the evaporated, single-blind, and large-scale samples were calculated by dividing the area under the chromatogram by the area under the chromatogram of the corresponding unevaporated sample.

For the evaporated and single-blind samples, the kinetic model was then applied to predict TICs and EIPs corresponding to each evaporation level for each liquid. To do this, the kinetic model was substituted into Eq. 4 to give the fraction remaining at a given retention index (F_{I^T}, Eq. 31)

$$F_{I^T} = \frac{C_{I^T,t}}{C_{I^T,0}} = exp(-exp(-1.05 \times 10^{-2} I^T + 6.71)\, t) \qquad \text{Eq. 31}$$

and the total fraction remaining (F_{Total}) was calculated according to Eq. 7. Predicted TICs and EIPs were subsequently generated by multiplying F_{I^T} by the abundance at the corresponding I^T in the TIC or corresponding EIP of the unevaporated liquid. To predict TICs and EIPs corresponding to different F_{Total} levels, *t* in Eq. 31 was varied until F_{Total} for the predicted chromatogram was equal to the F_{Total} level calculated for the experimental chromatogram. Experimental and predicted TICs and EIPs for the evaporated and single-blind samples were compared using PPMC coefficients (Eq. 11) to evaluate similarity, following procedures described in Section 1.1.6.

To identify liquids present in the large-scale burn samples, the experimental TICs and EIPs were compared to predicted reference collections of TICs and EIPs. The predicted chromatograms were generated as described above albeit varying *t* in Eq. 31 to reach F_{Total} levels ranging from 0.1 – 0.9 in increments of 0.1 (corresponding to evaporation levels ranging from 90 – 10% evaporated). The experimental TIC and relevant EIPs were compared to the corresponding predicted reference collection,

again using PPMC coefficients to evaluate similarity. In these comparisons, liquids present in the large-scale burn data were identified as the liquid in the reference collection to which the highest PPMC coefficient was observed.

4.1.5 Extension of iterative thermodynamic model to include the effect(s) of substrates

For the iterative thermodynamic model, we developed a procedure to examine the effect of substrates on the evaporation/weathering of the synthetic gasoline mixture. To test the extraction efficiencies, 1 mL of the gasoline mixture was spiked onto a 2" x 2" square of each substrate in a 250 mL glass jar. After 30 seconds, the substrates were then covered with pentane solvent for different periods of time to examine the effect of extraction time on the percent recoveries. For no substrate and cotton, 20 mL of pentane was added and equilibrium (i.e., maximum) efficiencies were achieved after ~30 seconds. For the nylon carpet sample, 50 mL pf pentane was added, and equilibrium conditions were established after 30 minutes. For pine wood and plywood, 70 mL of pentane were added, and equilibrium conditions were again reached after 30 minutes.

In the absence of any deliberate weathering, the relative proportion of each compound in the recovered residues was not significantly different from any of the substrates (Figure 12). However, the relative distribution of compounds was significantly different from the unweathered starting solution because of incidental headspace losses in the 250 mL jar during the liquid extraction, even though the jar was sealed for the duration of the liquid extraction. These results indicate that the liquid extraction procedure introduced slight evaporative losses to the headspace. We are currently in the process of accounting for these evaporative losses so that we can make confident assertions about the significance of the effect of substrate on the relative distribution of recovered compounds. We are confident that after accounting for headspace losses, there will not be any significant differences between the substrates.

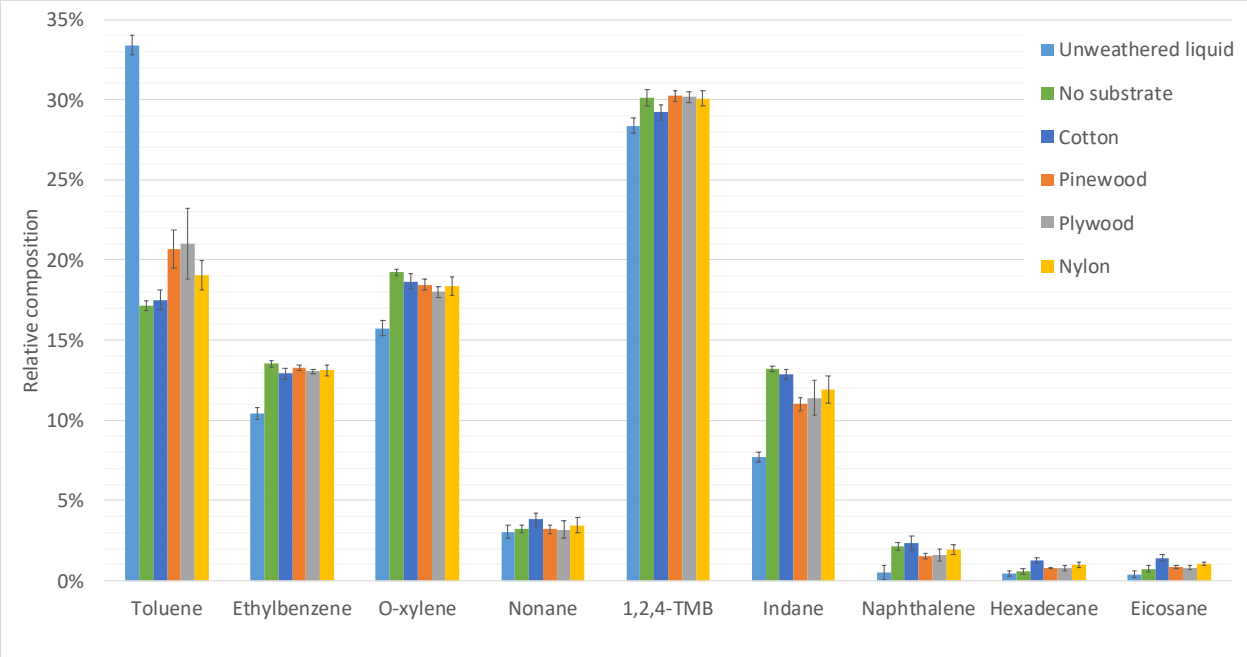

Figure 12. Fractional composition of the synthetic gasoline before and after applying the liquid extraction procedure in the absence of deliberate weathering. Error bars show 95% confidence interval for N=5 replicates.

This resource was prepared by the author(s) using Federal funds provided by the U.S. Department of Justice. Opinions or points of view expressed are those of the author(s) and do not necessarily reflect the official position or policies of the U.S. Department of Justice.

After establishing that the substrates have little or no effect on the recoveries, we then conducted weathering experiments of the synthetic gasoline from 0-95% at 210 °C in the presence of pine wood, plywood, cotton fabric and nylon carpet. In the presence of no substrate, the RMSEP of the (ideal) thermodynamic model was 1.6% (N=90). In the presence of cotton fabric (N=90) and nylon (N=72), the RMSEPs increased to 3% and 4%, respectively. In the presence of pinewood (N=99) and plywood (N=80), the RMSEPs increased to 6 and 8% respectively. Figure 13 shows the experimental data points and thermodynamic model predictions for the evaporation of the synthetic gasoline on cotton and pine wood at different extents of weathering. The results show that in the porous pine wood substrate, volatile compounds like toluene, ethylbenzene and o-xylene are present at much higher proportions than is predicted by the thermodynamic model.

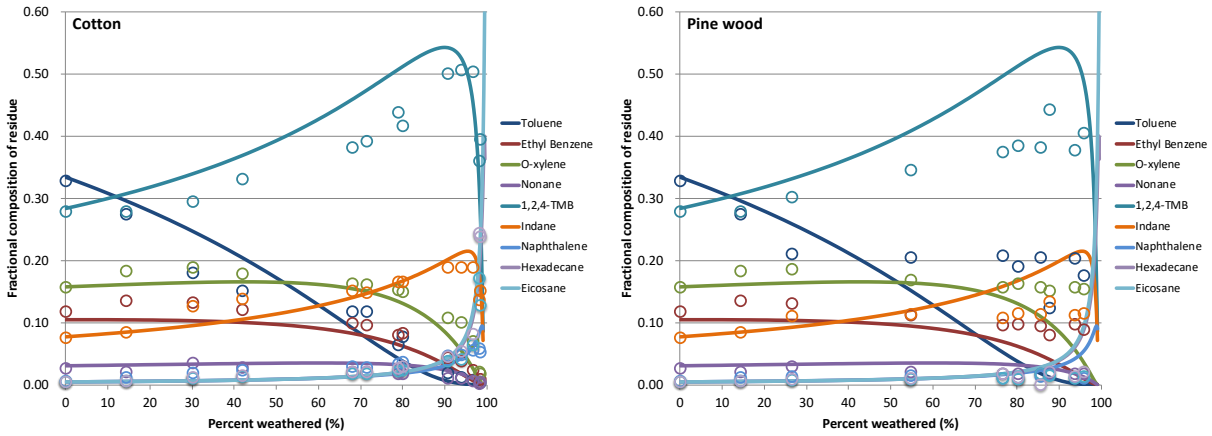

Figure 13. Fractional composition of the synthetic gasoline when weathered at 210 °C to different extents in the presence of cotton fabric and pine wood.

These results show that the presence of porous substrates has a significant effect on the weathering rates of volatile compounds, and that porous substrates help preserve the volatile components in the residues. In contrast, the non-volatile components evaporate faster than predicted by the model. These experiments help demonstrate that even when a liquid containing ~33% toluene has undergone 90% weathering at 210 °C, the residues can still contain up to 20% toluene in the residues if the substrate is highly porous, like pine wood. The same weathering conditions on an impervious substrate or minimally absorbent material like cotton fabric result in less than 0.1% toluene in the residues.

4.2 Results and Findings

4.2.1 Predicting TICs of liquids representing different ASTM classes

To this point, the kinetic model had primarily been used to predict evaporation of petroleum distillates and gasoline. However, it is important to demonstrate that the same model can be used to predict evaporation of liquids from different chemical classes. Without such ubiquity, the practicality of the model is limited as the identity of the liquid would need to be known for the correct model to be applied. The kinetic model was used to predict TICs corresponding to each of the experimentally evaporated liquids representing five different chemical classes defined in ASTM 1618 [4]. Representative predicted and experimental chromatograms for one liquid from the aromatic, isoparaffinic, naphthenic-paraffinic, and petroleum distillate classes are shown in Fig. 14, while predicted and experimental chromatograms corresponding to evaporated gasoline were shown in Fig. 9.

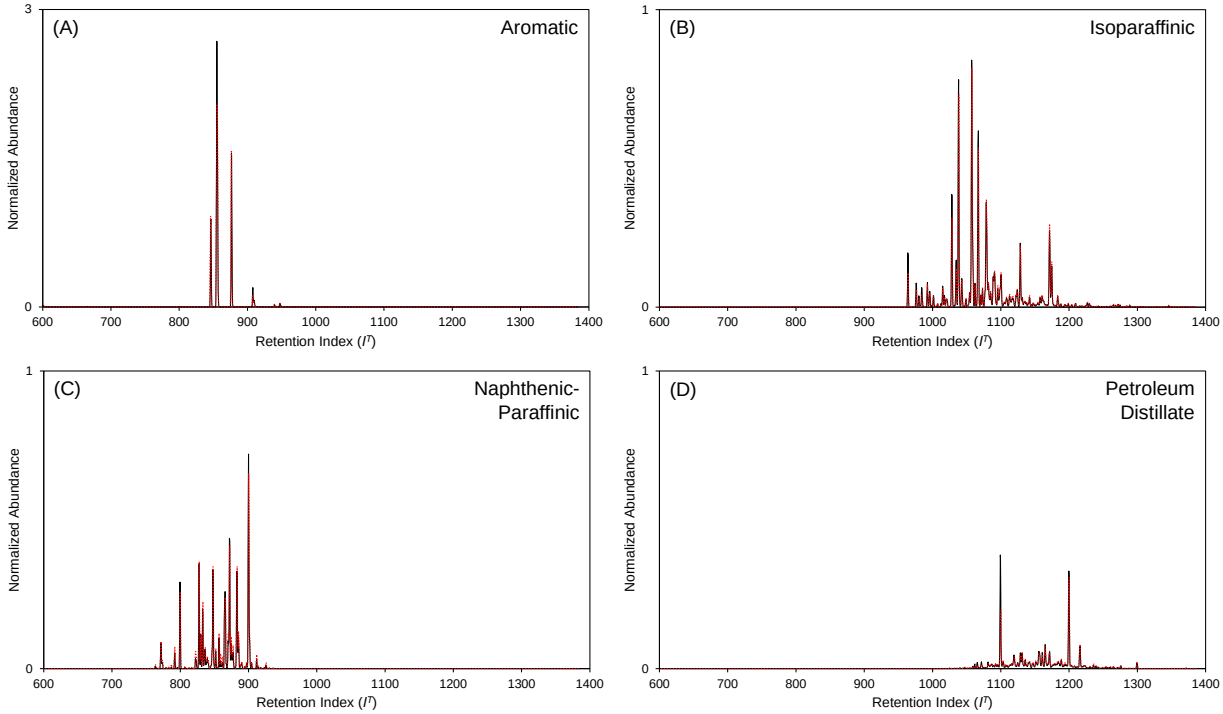

Figure 14. Predicted and experimental total ion chromatograms corresponding to F_{Total} = 0.3 for four liquids representing different ASTM classes (A) adhesive remover, aromatic class, (B) paint thinner, isoparaffinic class, (C) paint and varnish thinner, naphthenic-paraffinic class, and (D) lamp oil, petroleum distillate class. In each figure, experimental chromatograms are represented by the black solid line and predicted chromatograms are represented by the red dashed line.

Pearson product-moment correlation coefficients were calculated between the experimental and predicted TICs for each liquid at all F_{Total} levels (F_{Total} = 0.5, 0.3, and 0.1). Comparisons are shown in Table 9 for one liquid from each of the five classes while comparisons for the remaining liquids in each class are shown in Appendix 2, Tables A2.1 – A2.4.

For each liquid, comparisons of the predicted and experimental TICs indicated strong correlation with PPMC coefficients greater than 0.9 and, in many cases, greater than 0.98 (Table 9). For some liquids, there was a slight decrease in correlation as F_{Total} decreased (indicating higher levels of evaporation); however, in all cases, strong correlation was still observed. These findings were in agreement with previous comparisons of predicted and experimental TICs for gasoline and petroleum distillates and provide further evidence that the kinetic model can equally be applied to liquids representing a variety of chemical classes.

This resource was prepared by the author(s) using Federal funds provided by the U.S. Department of Justice. Opinions or points of view expressed are those of the author(s) and do not necessarily reflect the official position or policies of the U.S. Department of Justice.

Table 9. Mean PPMC coefficients for comparison of predicted and experimental TICs and EIPs corresponding to different chemical classes

Ignitable Liquid (ASTM Class)	F_{Total}	Mean PPMC coefficient for comparison of predicted and experimental TIC and EIPs					
		TIC	Alkane EIP	Cycloalkane EIP	Aromatic EIP	Indane EIP	PNA EIP
Adhesive remover (aromatic)	0.5	0.984 ± 0.007	-	-	0.98 ± 0.02	-	-
	0.3	0.972 ± 0.001	-	-	0.97 ± 0.01	-	-
	0.1	0.935 ± 0.005	-	-	0.90 ± 0.04	-	-
Gasoline (gasoline)	0.5	0.976 ± 0.002	0.973 ± 0.010	0.951 ± 0.019	0.975 ± 0.016	0.993 ± 0.004	0.995 ± 0.002
	0.3	0.993 ± 0.003	0.994 ± 0.001	0.965 ± 0.007	0.998 ± 0.001	0.994 ± 0.003	0.995 ± 0.002
	0.1	0.992 ± 0.001	0.966 ± 0.010	*	0.9941 ± 0.0003	0.992 ± 0.004	0.997 ± 0.001
Paint thinner (isoparaffinic)	0.5	0.984 ± 0.006	0.988 ± 0.003	0.989 ± 0.002	-	-	-
	0.3	0.9886 ± 0.0002	0.9883 ± 0.0004	0.990 ± 0.004	-	-	-
	0.1	0.933 ± 0.008	0.951 ± 0.008	0.89 ± 0.02	-	-	-
Paint & varnish thinner (naphthenic-paraffinic)	0.5	0.99 ± 0.02	0.99 ± 0.01	0.995 ± 0.004	-	-	0.990 ± 0.007
	0.3	0.97 ± 0.02	0.990 ± 0.004	0.992 ± 0.004	-	-	0.983 ± 0.005
	0.1	0.974 ± 0.005	0.980 ± 0.004	0.987 ± 0.004	-	-	0.981 ± 0.005
Lamp oil (petroleum distillate)	0.5	0.977 ± 0.003	0.992 ± 0.003	0.988 ± 0.001	-	-	-
	0.3	0.979 ± 0.001	0.988 ± 0.005	0.982 ± 0.001	-	-	-
	0.1	0.993 ± 0.007	0.992 ± 0.006	0.99 ± 0.01	-	-	-

- No EIP generated as profile class is not representative of the liquid

* No EIP predicted due to low abundance of compounds in the experimental EIP

4.2.2 Predicting EIPs of liquids representing different ASTM classes

For wider applicability of the kinetic model, it is also important to evaluate the model's suitability to predict extracted ion profiles (EIPs) representing different chemical classes for a given liquid. For each liquid analyzed, relevant EIPs were generated for the unevaporated and evaporated liquids in the instrument software. The kinetic model was then applied to the EIPs of the unevaporated liquids to predict EIPs corresponding to the F_{Total} levels of the evaporated liquids. As before, PPMC coefficients were used to evaluate the degree of similarity between the predicted and experimental EIPs. Comparisons of EIPs for one liquid from each ASTM class are shown in Table 9 while EIP comparisons for the remaining liquids in each class are shown in Appendix 2, Tables A2.1 – A2.4.

Similar to the trends observed for the TIC comparisons, there was strong correlation between the predicted and experimental EIPs, with PPMC coefficients greater than 0.9. For many liquids, coefficients for comparison of the predicted and experimental EIPs were often greater than those for the comparison of the corresponding TIC. It is worth noting that for the TIC comparisons, the extent of correlation depends on the presence of chromatographic peaks at corresponding I^T values and is independent of compound identity. While this is also fundamentally true for the EIPs, more chemical information is contained in the comparisons; that is, not only must a peak be present at the corresponding I^T value but the compound represented by the peak must also contain the same *m/z* values characteristic of the specific EIP.

4.2.3 Identifying liquids in single-blind samples

The next step to demonstrate practical utility of the kinetic model was to apply the model to determine the identity of an evaporated liquid in a single-blind sample. To do this, predicted TIC and EIP reference collections were generated to which the single-blind samples were compared. The kinetic model was first applied to the TIC of the unevaporated liquids, varying *t* in Eq. 31 to reach F_{Total} levels ranging from 0.1 – 0.9 in increments of 0.1 (corresponding to evaporation levels ranging from 90 – 10% evaporated). Relevant EIPs were then generated from each unevaporated liquid and the model applied in a similar

manner to generate a predicted reference collection containing F_{Total} levels ranging from 0.1 – 0.9 in increments of 0.1 for each EIP.

The TIC and each EIP from the single-blind samples were compared to the appropriate reference collection, calculating PPMC coefficients for each comparison. The liquid class was identified as the class to which highest correlation was observed. As an example, the TIC of blind sample A (Fig. 15A) was compared to the predicted TIC reference collection (Fig. 15B). The maximum correlation was observed for comparison to the predicted TIC of marine fuel stabilizer, a naphthenic-paraffinic, at $F_{Total} = 0.6$. Correlation to all other predicted TICs was less than 0.5, indicating weak correlation. As such, based on comparison of only the TIC, blind sample A was identified as a naphthenic-paraffinic liquid, which was the correct classification (Table 10).

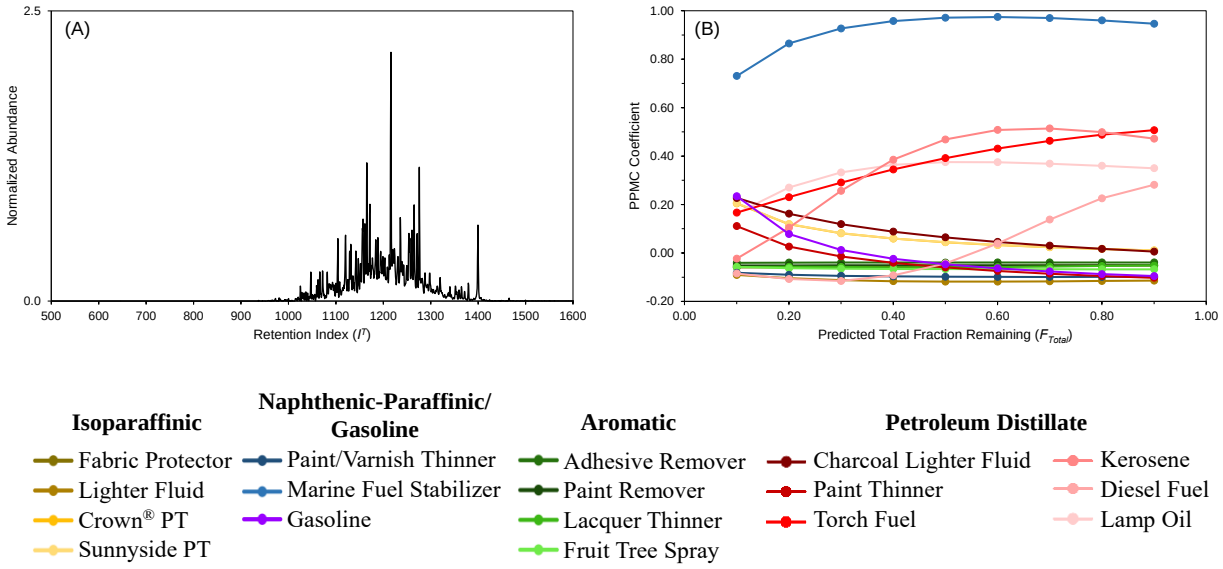

Figure 15. Identification of single blind sample A (A) TIC and (B) comparison to predicted TIC reference collection.

This resource was prepared by the author(s) using Federal funds provided by the U.S. Department of Justice. Opinions or points of view expressed are those of the author(s) and do not necessarily reflect the official position or policies of the U.S. Department of Justice.

Table 10. Identification of single-blind samples based on comparison to predicted TIC and EIP reference collections

Single-Blind Sample	Profile	Maximum Correlation			Actual Identity	
		PPMC coefficient	F_{Total}	Liquid Class	Liquid Class	F_{Total}
A	TIC	0.9743	0.6	Naphthenic-paraffinic	Naphthenic-paraffinic	0.6
B	TIC	0.9979	0.7	Petroleum distillate	Petroleum distillate	0.72
	Alkane	0.9977	0.8	Petroleum distillate		
	Cycloalkane	0.9973	0.7	Petroleum distillate		
C	TIC	0.9865	0.6	Naphthenic-paraffinic	Naphthenic-paraffinic	0.6
	Alkane	0.9827	0.7	Naphthenic-paraffinic		
	Cycloalkane	0.9907	0.6	Naphthenic-paraffinic		
	PNA	0.9821	0.8	Naphthenic-paraffinic		
D	TIC	0.8141	0.1	Aromatic	Aromatic	0.1
	Aromatic	0.9229	0.1	Aromatic		
E	TIC	0.8094	0.5	Aromatic	Miscellaneous	0.39
	Alkane	0.5360	0.3	Aromatic		
	Cycloalkane	0.6388	0.9	Isoparaffinic		
	Aromatic	0.8633	0.9	Aromatic		

For blind samples B – D, strong correlation was observed to more than one predicted TIC. For these samples, relevant EIPs were compared to the EIP reference collection and for all samples, the correct liquid class was identified (Table 10). For each liquid, the correct F_{Total} level was also determined although this is not necessary in fire debris analysis as the goal is to determine the liquid class present. For blind sample E, the TIC, alkane EIP, and aromatic EIP indicated the presence of an aromatic liquid whereas, the cycloalkane EIP indicated an isoparaffinic liquid (Table 10). Based on the liquid class definitions in ASTM 1618, aromatic liquids contain only aromatic compounds while the isoparaffinic class contains predominantly isoparaffinic compounds with minimal to no aromatics. From the TIC and EIPs of blind sample E, the sample contains both aromatic and isoparaffinic compounds and therefore, cannot be classified exclusively into one class. The ASTM standard also includes a miscellaneous class, which is reserved for liquids that contain compounds spanning more than one class and therefore, cannot be represented by a single class. Based on the presence of both aromatic and isoparaffinic compounds, blind sample E was classified as a miscellaneous liquid.

The single-blind samples serve to demonstrate the utility of predicted reference collections. Blind samples A – C were liquids already present in the reference collection and therefore demonstrated same-source comparisons. Blind sample D was a liquid not included in the reference collection but for which the liquid class was represented in the collection. As such, blind sample D represented a different-source comparison which is more realistic given that debris samples submitted to a laboratory are unlikely to contain the same liquid as in the laboratory reference collection. Finally, blind sample E was a liquid for which neither liquid nor class was represented in the reference collection. Nonetheless, an identification was still possible based on knowledge of the classes present in the liquid.

4.2.4 Identifying liquids in large-scale burns

Debris samples collected from three large-scale burns were analyzed by GC-MS. These represent the most realistic samples analyzed and as expected, the TICs indicated the presence of substrate

interferences, which ranged from minor contributions (burn sample A) to major contributions (burn sample C). The TICs and the relevant EIPs from each burn sample were compared to the predicted reference collections for identification. Comparisons of the TIC and relevant EIPs from each burn sample to the corresponding predicted reference collections are summarized in Table 11 and discussed in more detail in the following paragraphs.

The TIC of burn sample A was dominated by *n*-alkanes in the range $C_{12} - C_{15}$ with minor contributions from styrene ($I^T = 871$) and methylstyrene ($I^T = 978$) (Fig. 16A). Styrene and methylstyrene were identified as substrate interferences based on their presence chromatograms of the burned carpet alone. When compared to the predicted TIC reference collection, maximum correlation (r = 0.8626) was observed for comparison to torch fuel, which is a petroleum distillate (Fig. 16B). Extracted ion profiles corresponding to the alkane and cycloalkane classes were also generated from burn sample A and compared to the predicted EIP reference collection (Appendix 3). For both EIPs, maximum correlation was observed for comparisons to torch fuel (r = 0.8486 and 0.9069, respectively). Thus, the liquid present in burn sample A was identified as a petroleum distillate, similar to torch fuel.

Table 11. Identification of ignitable liquid in large-scale burn samples based on comparison of TICs and EIPs to corresponding predicted TIC and EIP reference collections.

Burn Sample	Profile	Comparison to Predicted Reference Collection		Actual Liquid Class
		Max. PPMC coefficient	Liquid Class	
A	TIC	0.8626	Pet. distillate	Pet. distillate
	Alkane EIP	0.8486	Pet. distillate	
	Cycloalkane EIP	0.9069	Pet. distillate	
B	TIC	0.8389	Gasoline	Gasoline
	Alkane EIP	0.8629	Gasoline	
	Aromatic EIP	0.8686	Gasoline	
	Indane EIP	0.9021	Gasoline	
	PNA EIP	0.8283	Aromatic	
C	TIC	-	-	Gasoline
	Alkane EIP	0.5336	Gasoline	
	Aromatic EIP	0.3370	Gasoline	
	Indane EIP	0.5880	Gasoline	

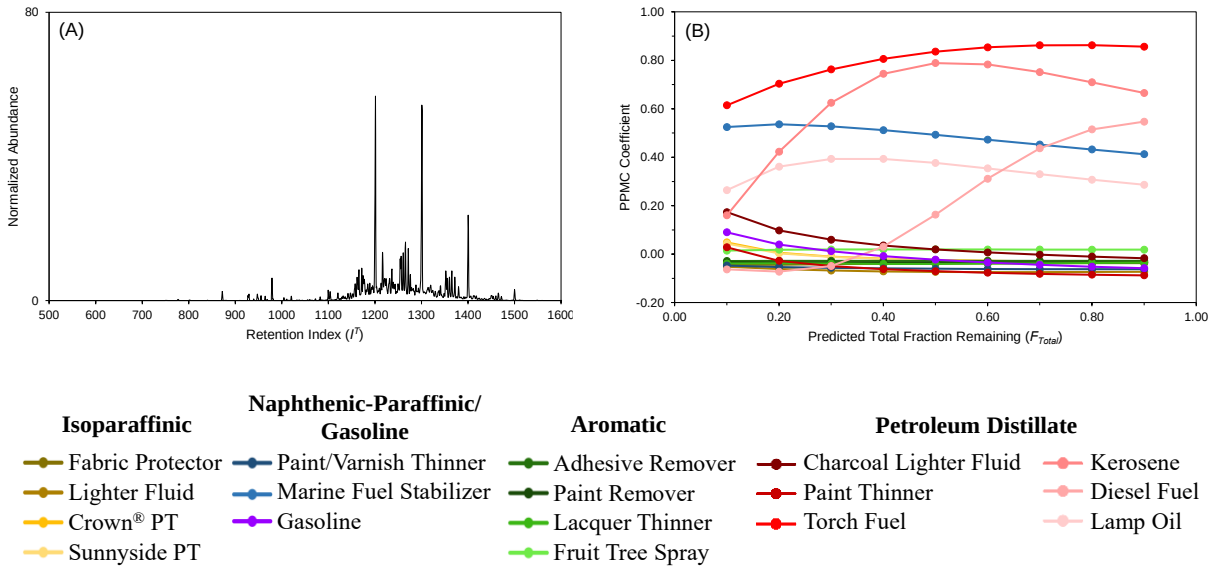

Figure 16. Identification of ignitable liquid in large-scale burn samples (A) TIC of burn sample A and (B) comparison of TIC to predicted TIC reference collection.

The TIC of burn sample B indicated the presence of toluene (I^T = 749), C_2-alkylbenzenes (I^T = 749), C_2-alkylbenzenes (I^T = 845–875), C_3-alkylbenzenes (I^T = 947–1004), and 1-methylnaphthalene (I^T = 1284), which are compounds expected in gasoline (Fig. 17A). However, toluene and the C_2-alkylbenzenes were present at relatively low abundance and the TIC also contained moderate contributions from styrene (I^T = 863) and estragole (I^T = 1170). On comparison to the predicted TIC reference collection, maximum correlation (r = 0.8389) was observed for comparison to gasoline (Fig. 17B).

The alkane, aromatic, and indane EIPs also indicated maximum correlation to gasoline (r = 0.8629, 0.8686, and 0.9021, respectively) (Appendix 4). In contrast, the PNA EIP (Fig. 17C) indicated maximum correlation to fruit tree spray (r = 0.8283), which is an aromatic liquid (Fig. 17D). Maximum correlation was due to the high abundance of naphthalene in the PNA profile of both fruit tree spray and burn sample B. Naphthalene was also present in high abundance in the PNA profile of burned carpet (Appendix 3), indicating that the presence of this compound in burn sample B was primarily due to substrate interferences. Thus, based on the TIC, alkane EIP, aromatic EIP, and indane EIP, the liquid in burn sample B was identified as gasoline. The alkane, aromatic, and indane EIPs contained minimal or no substrate interferences, increasing the utility of these profiles for identification of the liquid. In contrast, the PNA profile contained primarily substrate contributions thereby limiting the use of this profile for identification.

This resource was prepared by the author(s) using Federal funds provided by the U.S. Department of Justice. Opinions or points of view expressed are those of the author(s) and do not necessarily reflect the official position or policies of the U.S. Department of Justice.

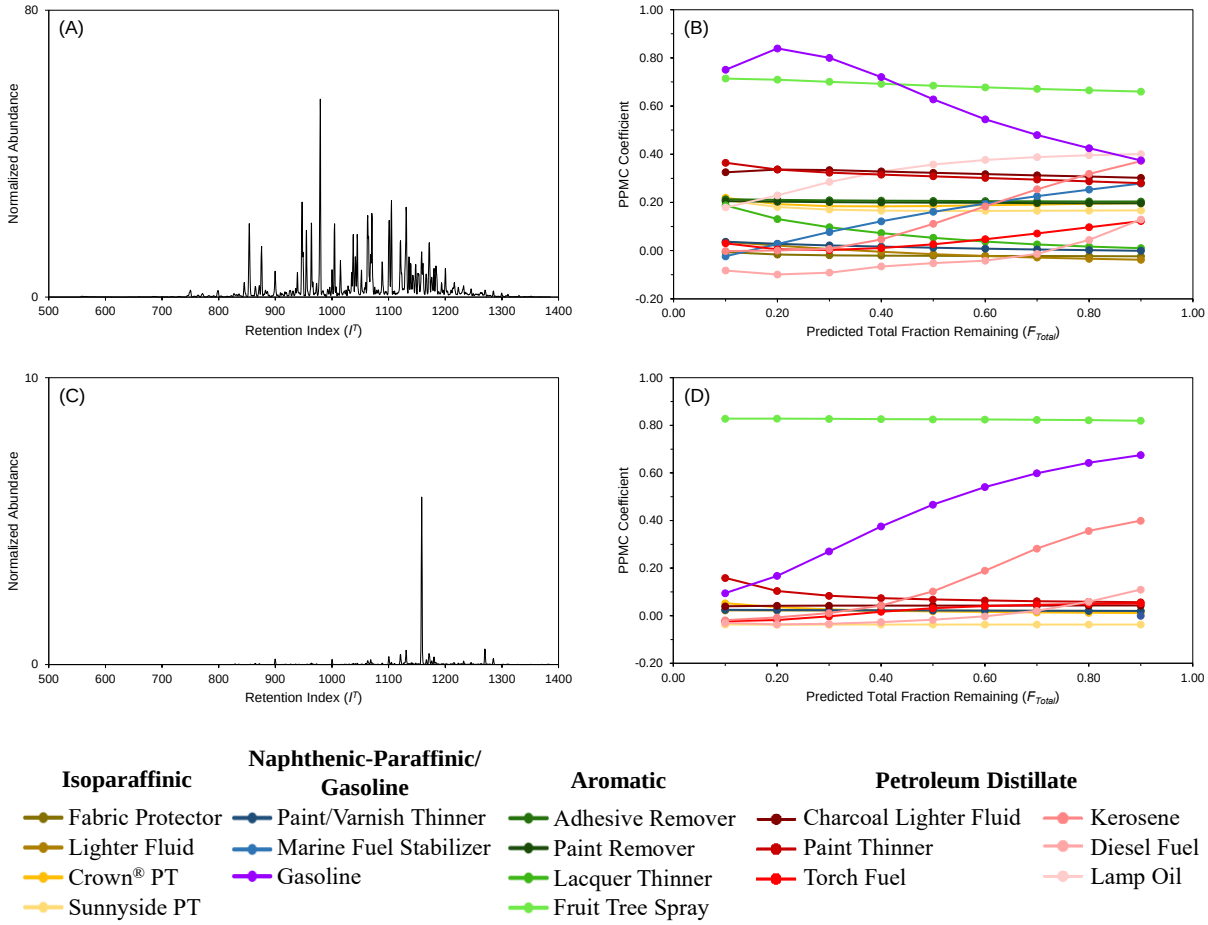

Figure 17. Identification of ignitable liquid in large-scale burn samples (A) TIC of burn sample B, (B) comparison of TIC to predicted TIC reference collection, (C) PNA EIP of burn sample B, and (D) comparison of PNA EIP to predicted EIP reference collection.

The TIC of burn sample C was dominated by trimethylbicycloheptene (I^T = 930) and β-pinene (I^T = 968), with minor contributions from hexanal, nonanal, decanal, and C_2- and C_4-alkylbenzenes (Fig. 18A). With the exception of the alkylbenzenes, all compounds were also present in the TIC of unburned wood flooring. Given the abundance of these substrate interferences, the TIC was defined as containing major substrate interferences. When compared to the predicted TIC reference collection, there was no correlation to any liquid, with $r < 0.2$ for all comparisons (Fig. 18B).

The alkane EIP was dominated by the aliphatic aldehydes as these substrate interferences contained the same ions used to generate the alkane profile (Appendix 5). Similarly, the aromatic EIP contained trimethylbicycloheptene and β-pinene as these compounds contain the same ions as used to generate the profile (Appendix 4). When the alkane and aromatic EIPs were compared to the predicted reference collection, maximum correlation was observed for comparison to gasoline (r = 0.5336 and 0.3370, respectively); however, this maximum correlation indicated only moderate to weak correlation, which was expected given the presence of substrate interferences in the EIPs (Appendix 5). In contrast, the indane EIP (Fig. 18C), which did not contain substrate contributions, yielded a higher maximum correlation (r = 0.5880) to gasoline (Fig. 18D). Although gasoline could not be definitively identified in

This resource was prepared by the author(s) using Federal funds provided by the U.S. Department of Justice. Opinions or points of view expressed are those of the author(s) and do not necessarily reflect the official position or policies of the U.S. Department of Justice.

this sample due to the extensive nature of the substrate interferences, comparison of the EIPs to the predicted reference collection did indicate the possible presence of gasoline.

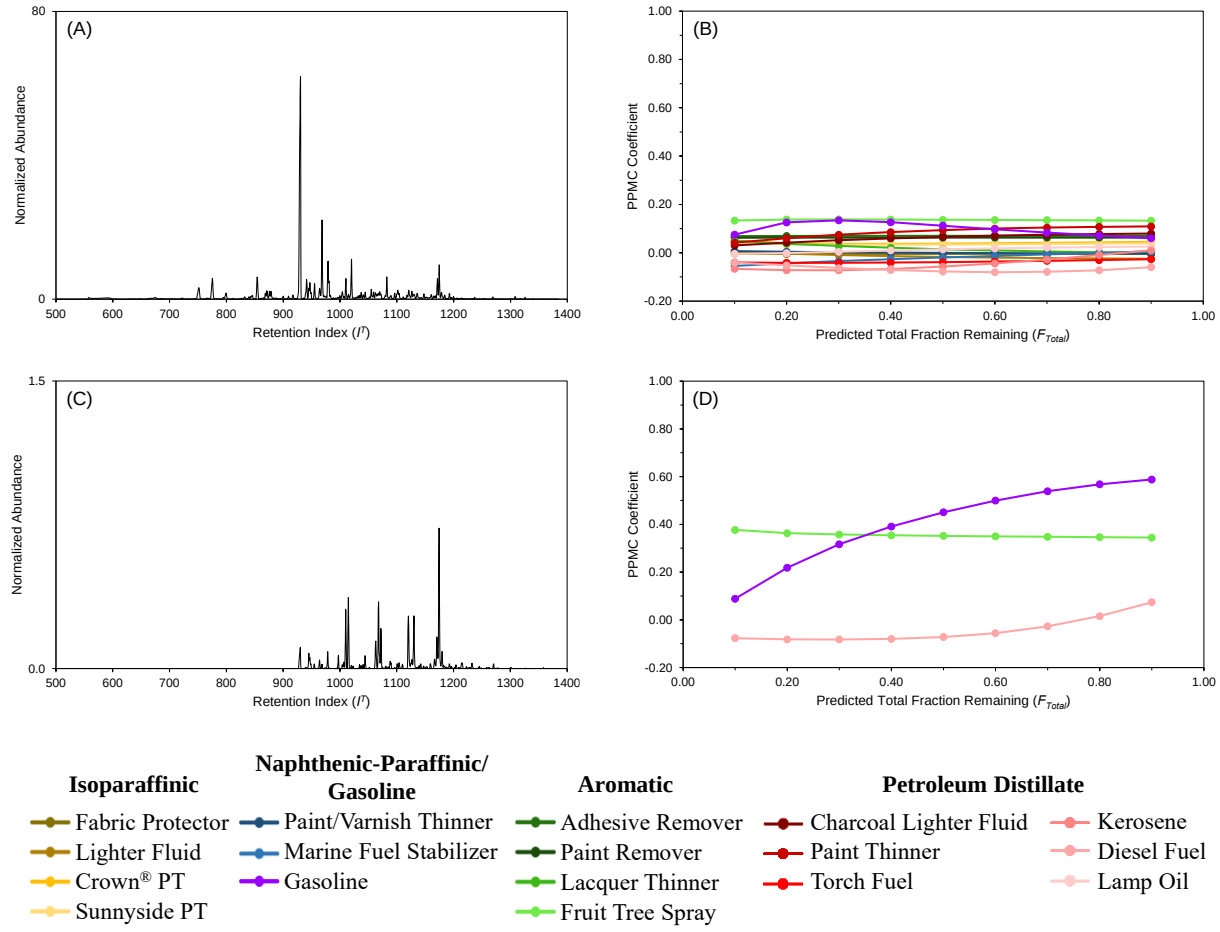

Figure 18. Identification of ignitable liquid in large-scale burn samples (A) TIC of burn sample C, (B) comparison of TIC to predicted TIC reference collection, (C) indane EIP of burn sample C, and (D) comparison of indane EIP to predicted EIP reference collection.

4.3 Activities and Accomplishments

Peer-reviewed publications

Eklund NK, Capistran BA, McGuffin VL, Waddell Smith R. Improvements in a Kinetic-Based Model to Predict Evaporation of Gasoline. *Forensic Chemistry* **2020**, *17*, 100194. https://doi.org/10.1016/j.forc.2019.100194.

Capistran BA, McGuffin VL, Waddell Smith R. Application of a Kinetic Model to Predict Extracted Ion Profiles for the Identification of Evaporated Ignitable Liquids. *Forensic Chemistry* **2021**, *24*, 100340. https://doi. org/10.1016/j.forc.2021.100340.

*Conference presentations (presenting author underlined, † indicates graduate student, †† indicates undergraduate student, * indicates invited presentation)*

†Briana A. Capistran, Victoria L. McGuffin, and Ruth Waddell Smith. Generating Reference Collections of Evaporated Liquids using a Kinetic-Based Model. Oral presentation at the 48th Annual Meeting of the Midwestern Association of Forensic Scientists, Louisville, KY. October 2019.

†Briana A. Capistran, Victoria L. McGuffin, and Ruth Waddell Smith. Practical Application of a Kinetic Model to Generate Predicted Reference Collections for the Identification of Ignitable Liquids in Fire Debris Samples. Oral presentation at the 72nd American Academy of Forensic Sciences Annual Meeting, Anaheim, CA. February 2020.

†Briana A. Capistran, Victoria L. McGuffin, and Ruth Waddell Smith. Practical Application of a Kinetic Model to Generate Predicted Reference Collections for the Identification of Ignitable Liquids in Fire Debris Samples. Oral presentation at the 72nd American Academy of Forensic Sciences Annual Meeting, Anaheim, CA. February 2020.

Theses

Capistran, BA. Kinetically Modeling Total Ion Chromatograms and Extracted Ion Profiles to Identify Ignitable Liquids for Fire Debris Applications. MS Thesis, **2020**, Michigan State University, East Lansing, MI.

4.4 Limitations and Areas of Future Work

The practical application of the kinetic model for fire debris analysis was demonstrated in this goal. The model was used to generate predicted reference collections of TICs and EIPs which were subsequently used to successfully identify the class of liquid present in a series of single-blind samples and large-scale burn samples. While the fixed-temperature kinetic model at 20 °C was used in this goal, the model was effective in identifying evaporated liquids in the large-scale burn samples, which were subjected to significantly higher temperatures. However, a more comprehensive evaluation of model performance at higher temperatures is needed and will be the focus of future work. The effect of substrates on evaporation rates will also be evaluated more thoroughly. A preliminary evaluation was performed during this project in which diesel was evaporated from different substrates (glass, nylon, polyester, and cotton). Evaporation rate constants for selected compounds were experimentally determined and models were developed for each substrate. However, there was no significant difference in regression coefficients for each substrate model. Future work will re-evaluate the effect of substrates on evaporation, focusing on both surface porosity and surface chemistry of the substrate.

Participants and other collaborating organizations

Michigan State University

Principal Investigators:	Ruth Waddell Smith Victoria L. McGuffin
Graduate Students:	Amanda (Setser) Burkhart Briana Capistran Hannah Lavoie William Shirley

West Virginia University

Principal Investigator:	Glen P. Jackson
Undergraduate Students:	Evan Ferweda Ahna Kotula Hannah McMillen Isaac Willis
Graduate Students:	J. Tyler Davidson Max Denn Caitlyn (Lear) Wensel

Artifacts

Conference Presentations

*(*denotes invited presentation; † denotes graduate student; †† denotes undergraduate student; presenter underlined)*

1. ††Isaac C. Willis, Zilin Fan, †J. Tyler Davidson, Glen P. Jackson. The Influence of Elevated Temperatures on the Weathering of Ignitable Liquids. Poster presentation at the Pittsburgh Conference on Analytical Chemistry and Applied Spectroscopy, Philadelphia, PA, March 2019. (NIJ Poster session)
2. †Briana A. Capistran, Victoria L. McGuffin, and Ruth Waddell Smith. Generating Reference Collections of Evaporated Liquids using a Kinetic-Based Model. Oral presentation at the 48th Annual Meeting of the Midwestern Association of Forensic Scientists, Louisville, KY. October 2019.
3. Victoria L. McGuffin and Ruth Waddell Smith. Kinetic and Thermodynamic Models of Evaporation for Forensic Applications. Oral presentation at the SciX Conference, Palm Springs, CA. October 2019.
4. †Amanda L. Setser, Victoria L. McGuffin, and Ruth Waddell Smith. Refinement and Application of a Kinetic Model to Predict Evaporation of Gasoline for Fire Debris Analysis. Oral presentation at the 72nd American Academy of Forensic Sciences Annual Meeting, Anaheim, CA. February 2020.
5. †Caitlyn Wensel, ††Isaac Willis, Zilin Fan, †J. Tyler Davidson, and Glen P. Jackson. The Effects of Elevated Temperatures and Substrates on the Weathering of Ignitable Liquids. Oral presentation at the 72nd American Academy of Forensic Sciences Annual Meeting, Anaheim, CA. February 2020.

6. †Briana A. Capistran, Victoria L. McGuffin, and Ruth Waddell Smith. Practical Application of a Kinetic Model to Generate Predicted Reference Collections for the Identification of Ignitable Liquids in Fire Debris Samples. Oral presentation at the 72nd American Academy of Forensic Sciences Annual Meeting, Anaheim, CA. February 2020.
7. †Caitlyn Wensel, ††Isaac C. Willis, Zilin Fan, †J. Tyler Davidson, †Natasha K. Eklund, †Amanda L. Setser, Victoria L. McGuffin, Ruth Waddell Smith, and Glen P. Jackson. Thermodynamic and Kinetic Predictions of the Evaporation Patterns of Ignitable Liquids at Elevated Temperatures. Oral presentation at the 71st Annual Pittsburgh Conference on Analytical Chemistry and Applied Spectroscopy (Pittcon), Chicago, IL. March 2020.
8. *†Briana A. Capistran, Victoria L. McGuffin, and Ruth Waddell Smith. Practical Application of a Kinetic Model to Identify Evaporated Ignitable Liquids in Fire Debris Samples. Oral presentation at the SciX Conference (virtual). October 2020.
9. ††Evan Ferweda, ††Ahna Kotula, †Caitlyn Wensel, Glen P. Jackson. Simulating Weathering of Ignitable Liquids to Understand the Effect of Mole Fraction on Weathering. Poster Presentation at the 2020 Undergraduate Research Symposium, Morgantown, WV (virtual), April 2020.
10. *†Amanda L. (Setser) Burkhart, Victoria L. McGuffin, and Ruth Waddell Smith. Predicting Evaporation of Volatile Compounds in Gasoline using a Refined Kinetic Model. Oral presentation at the 72nd Annual Pittsburgh Conference on Analytical Chemistry and Applied Spectroscopy (Pittcon, virtual). March 2021.
11. ††Hannah L. McMillen, Glen P. Jackson. Evaluation of a Thermodynamic Model to Predict the Weathering of Ignitable liquids at Elevated Temperatures. Oral presentation at the 74th American Academy of Forensic Sciences Annual Meeting, Seattle, WA. February 2022.
12. ††Ahna Kotula, †Caitlyn Wensel, Glen P. Jackson. The Effects of Substrates and Elevated Temperatures on the Weathering of Ignitable Liquids. Poster presentation at the Chesapeake Bay Division of the International Association for Identification, Gaithersburg, MD. March 2022.
13. ††Hannah McMillen, Glen P. Jackson. The Evaluation of a Thermodynamic Model to Predict the Weathering of Ignitable Liquids at Different Temperatures. Poster (virtual) presentation at the Pittsburgh Conference on Analytical Chemistry and Applied Spectroscopy, Atlanta, GA. March 2022.

Publications

1. Eklund NK, Capistran BA, McGuffin VL, Waddell Smith R. Improvements in a Kinetic-Based Model to Predict Evaporation of Gasoline. *Forensic Chemistry* **2020**, *17*, 100194. https://doi.org/10.1016/j.forc.2019.100194.
2. Willis IC, Fan Z, Davidson JT, Jackson GP. Weathering of Ignitable Liquids at Elevated Temperatures: A Thermodynamic Model, Based on Laws of Ideal Solutions, to Predict Weathering in Structure Fires. *Forensic Chemistry* **2020**, *18*, 100215. https://doi.org/10.1016/j.forc.2020.100215.
3. McGuffin VL, Waddell Smith R. A Unified Kinetic and Thermodynamic Model of Evaporation for Forensic Applications. *Forensic Chemistry* **2021**, *23*, 100304. https://doi.org/10.1016/j.forc.2020.100304.
4. Capistran BA, McGuffin VL, Waddell Smith R. Application of a Kinetic Model to Predict Extracted Ion Profiles for the Identification of Evaporated Ignitable Liquids. *Forensic Chemistry* **2021**, *24*, 100340. https://doi. org/10.1016/j.forc.2021.100340 .

5. Burkhart AL, Waddell Smith R, McGuffin VL. Measuring Evaporation Rate Constants of Highly Volatile Compounds for Use in Predictive Kinetic Models. *Analytica Chimica Acta* 1182, **2021**, 338932. https://doi.org/10.1016/j.aca.2021.338932.
6. McGuffin VL, Waddell Smith R. A Kinetic Model of Evaporation Based on Gas Chromatographic Retention Index: Environmental and Forensic Applications. *Advances in Chromatography*. In press.
7.

Theses

1. Wensel C. The Effects of Household Substrates on the Evaporation of Ignitable Liquids at Temperatures up to 210 °C. MS Thesis, **2020**, West Virginia University, Morgantown, WV.
2. Capistran, BA. Kinetically Modeling Total Ion Chromatograms and Extracted Ion Profiles to Identify Ignitable Liquids for Fire Debris Applications. MS Thesis, **2020**, Michigan State University, East Lansing, MI.
3. Burkhart, AL. Measuring Evaporation Rate Constants of Highly Volatile Compounds and Investigating the Effect of Interface on a Kinetic Model Applied to Forensic Fire Debris. PhD Thesis, **2021**, Michigan State University, East Lansing, MI.

References

[1] ASTM E1386-15: Standard practice for separation of ignitable liquid residues from fire debris samples by solvent extraction, ASTM International, West Conshohocken, PA, 2015.
[2] ASTM E2154-15a: Standard practice for separation and concentration of ignitable liquid residues from fire debris samples by passive headspace concentration with solid phase microextraction (SPME), ASTM International, West Conshohocken, PA, 2015.
[3] ASTM E1413-19: Standard practice for separation of ignitable liquid residues from fire debris samples by dynamic headspace concentration onto an adsorbent tube, ASTM International, West Conshohocken, PA, 2019.
[4] ASTM E1618-19: Standard test method for ignitable liquid residues in extracts from fire debris samples by gas chromatography-mass spectrometry, ASTM International, West Conshohocken, PA, 2019.
[5] ASTM E1412-19: Standard practice for separation of ignitable liquid residues from fire debris samples by passive headspace concentration with activated charcoal, ASTM International, West Conshohocken, PA, 2019.
[6] Ignitable Liquids Reference Collection Database. National Center for Forensic Science, University of Central Florida.
[7] S.S. Hetzel, Survey of American gasolines (2008), Journal of Forensic Sciences 60 (2015) S197-S206.
[8] R. Hirz, Gasoline brand identification and individualization of gasoline lots, Journal of Forensic Sciences 29 (1989) 91-101.
[9] P.M.L. Sandercock, E. Du Pasquier, Chemical fingerprinting of gasoline. 2. Comparison of unevaporated and evaporated automotive samples, Forensic Science International 140 (2004) 43-59.
[10] A. Berry, T. Dabrowski, K. Lyons, The oil spill model OILTRANS and its application to the Celtic Sea, Marine Pollution Bulletin 64 (2012) 2489-2501.
[11] M.F. Fingas, Studies on the evaporation of crude oil and petroleum products: I. The relationship between evaporation rate and time, Journal of Hazardous Materials 56 (1997) 227-236.
[12] M.F. Fingas, Studies on the evaporation of crude oil and petroleum products: II. Boundary layer regulation, Journal of Hazardous Materials 57 (1998) 41-58.
[13] M.F. Fingas, Modeling evaporation using models that are not boundary-layer regulated, Journal of Hazardous Materials 107 (2004) 27-36.
[14] R.K. Jones, Method for estimating boiling temperatures of crude oils, Journal of Environmental Engineering 122 (1996) 761-763.
[15] W. Lehr, R.K. Jones, M. Evans, D. Simecek-Beatty, R. Overstreet, Revisions of the ADIOS oil spill model, Environmental Modelling & Software 17 (2002) 191-199.
[16] D. Mackay, R.S. Matsugu, Evaporation rates of liquid hydrocarbon spills on land and water, The Canadian Journal of Chemical Engineering 51 (1973) 434-439.
[17] W. Stiver, D. Mackay, Evaporation rate of spills of hydrocarbons and petroleum mixtures, Environmental Science and Technology 18 (1984) 834-840.
[18] H.L. Birks, A.R. Cochran, T.J. Williams, G.P. Jackson, The surprising effect of temperature on the weathering of gasoline, Forensic Chemistry 4 (2017) 32-40.
[19] J.W. McIlroy, A.D. Jones, V.L. McGuffin, Gas chromatographic retention index as a basis for predicting evaporation rates of complex mixtures, Analytica Chimica Acta 852 (2014) 257-266.
[20] R. Waddell Smith, R.J. Brehe, J.W. McIlroy, V.L. McGuffin, Mathematically modeling chromatograms of evaporated ignitable liquids for fire debris applications, Forensic Chemistry 2 (2016) 37-45.
[21] J.W. McIlroy, R. Waddell Smith, V.L. McGuffin, Fixed- and variable-temperature kinetic models to predict evaporation of petroleum distillates for fire debris applications, Separations 5 (2018) 47.
[22] N.K. Eklund, B.A. Capistran, V.L. McGuffin, R. Waddell Smith, Improvements in a kinetic-based model to predict evaporation of gasoline, Forensic Chemistry 17 (2020) 100194.

[23] J.L. DeVore, Probability and Statistics for Engineering and the Sciences, Duxbury Press, Belmont, CA, 1990.
[24] I.C. Willis, Z. Fan, J.T. Davidson, G.P. Jackson, Weathering of ignitable liquids at elevated temperatures: A thermodynamic model, based on laws of ideal solutions, to predict weathering in structure fires, Forensic Chemistry 18 (2020) 100215.
[25] C.L. Yaws, P. Narasimhan, C. Gabbula, Yaws' Handbook of Antoine Coefficients for Vapor Pressure., 2009.
[26] P. Atkins, J. dePaula, Physical Chemistry, 9th ed., W.H. Freeman and Company, New York, NY, 2009.
[27] NIST Chemistry WebBook, SRD 69.
[28] B.E. Poling, J.M. Prausnitz, J.P. O'Connell, Properties of Gases and Liquids, 5th ed., McGraw-Hill, New York, NY, 2001.

Appendices

Appendix 1. Percent error in prediction using fixed-and variable-temperature kinetic and thermodynamic models based on three compound classes.

Table A1.1 Percent error in predicting rate constant using fixed-temperature kinetic models

Compound	Retention Index (I^T)[a]	Percent Error in Predicting Rate Constant[c]				
		5 °C[d]	10 °C[e]	20 °C[f]	30 °C[g]	35 °C[h]
Octane	800	12.85	-1.12	7.43	2.80	-6.63
Nonane	900	28.10	31.43	20.42	15.79	23.13
Decane	1000	24.26	28.97	28.65	25.55	36.76
Undecane	1100	19.94	0.10	13.13	15.54	21.41
Dodecane	1200			25.20	15.25	6.85
Tridecane	1300			83.45	7.57	-2.56
Toluene	750	-12.70	-25.36	-12.55	-11.90	-24.26
Ethylbenzene	844	-12.82	-7.41	-12.74	-10.82	-14.38
Propylbenzene	938	-8.34	2.68	-6.54	-9.47	-2.18
Butylbenzene	1040	-11.47	-7.89	-5.04	-2.02	5.19
Pentylbenzene	1141	-16.80	-27.13	-20.77	-9.90	-10.37
m-,*p*-Xylene	853	2.15	10.15	-0.65	1.27	-4.22
o-Xylene	876	-1.89	5.43	-6.61	-5.22	-6.30
Ethylmethylbenzene isomer	945	2.26	14.78	2.95	-4.23	9.25
Ethylmethylbenzene isomer	962	-0.38	9.85	-1.06	-3.13	6.54
Methylpropylbenzene isomer	1036	-4.56	-1.64	-2.37	-0.06	8.88
Methylpropylbenzene isomer	1050	-10.07	-12.03	-8.24	-5.07	2.07
1,3,5-Trimethylbenzene	953	26.14	35.88	18.30	15.25	23.36
1,2,4-Trimethylbenzene	978	1.00	14.44	3.71	0.43	12.93
Methylcyclohexane	719[b]	-12.05	-23.48	-3.16	-4.55	-20.82
Ethylcyclohexane	828	-1.21	-5.20	-1.96	0.93	-8.59
Propylcyclohexane	925	5.92	10.43	2.20	2.80	11.18
Butylcyclohexane	1027	-3.54	1.12	4.44	6.49	13.66
Pentylcyclohexane	1130	-8.87	-21.57	-11.95	-0.41	-0.89
Hexylcyclohexane	1241			-14.69	-14.07	-13.63
Heptylcyclohexane	1338				-15.71	-33.56
Mean Absolute Percent Error (%)		**10.33**	**13.55**	**12.73**	**7.93**	**12.68**
Overall Mean Absolute Percent Error (%)		**11.40**				

[a]Retention indices experimentally determined by McIlroy *et al.* [19]
[b]Retention index from [27]
[c]Percent error calculated as: % error = $((k_{pred} - k_{experimental})/k_{experimental}) \times 100$
[d]Rate constants at 5°C predicted using fixed-temperature model at 5°C, coefficients shown in Table 7.
[e]Rate constants at 10°C predicted using fixed-temperature model at 10°C, coefficients shown in Table 7.
[f]Rate constants at 20°C predicted using fixed-temperature model at 20°C, coefficients shown in Table 7.
[g]Rate constants at 30°C predicted using fixed-temperature model at 30°C, coefficients shown in Table 7.
[h]Rate constants at 35°C predicted using fixed-temperature model at 35°C, coefficients shown in Table 7.

Table A1.2 Percent error in predicting rate constant using variable-temperature kinetic model

Compound	Retention Index (I^T)[a]	Percent Error in Predicting Rate Constant[c]				
		5 °C[d]	10 °C[e]	20 °C[f]	30 °C[g]	35 °C[h]
Octane	800	-20.14	-0.69	37.29	12.91	-15.47
Nonane	900	-0.38	40.66	53.49	22.96	8.32
Decane	1000	6.18	47.11	63.55	28.90	16.92
Undecane	1100	12.63	21.68	43.44	14.69	0.87
Dodecane	1200			58.32	10.61	-13.74
Tridecane	1300			131.37	-0.18	-23.55
Toluene	750	-41.06	-27.39	11.91	-1.60	-30.44
Ethylbenzene	844	-35.69	-4.38	11.39	-3.50	-23.46
Propylbenzene	938	-26.12	12.59	19.01	-5.09	-14.88
Butylbenzene	1040	-21.45	7.77	20.59	-0.76	-11.10
Pentylbenzene	1141	-18.80	-9.08	0.35	-11.79	-26.40
m-,p-Xylene	853	-24.01	14.41	26.79	9.25	-14.60
o-Xylene	876	-25.41	11.13	19.12	1.47	-17.00
Ethylmethylbenzene isomer	945	-17.03	26.41	31.07	0.17	-5.12
Ethylmethylbenzene isomer	962	-17.87	22.30	25.90	0.73	-7.92
Methylpropylbenzene isomer	1036	-15.63	14.79	23.99	1.37	-7.87
Methylpropylbenzene isomer	1050	-19.44	3.59	16.49	-4.17	-13.98
1,3,5-Trimethylbenzene	953	3.11	50.42	50.58	20.22	6.89
1,2,4-Trimethylbenzene	978	-15.47	28.72	31.92	3.87	-2.85
Methylcyclohexane	719[b]	-42.33	-27.02	24.02	7.73	-26.64
Ethylcyclohexane	828	-28.22	-3.08	25.20	9.81	-17.91
Propylcyclohexane	925	-15.67	20.09	30.18	8.24	-2.89
Butylcyclohexane	1027	-15.45	17.34	32.68	8.34	-3.58
Pentylcyclohexane	1130	-11.98	-2.82	11.55	-2.14	-18.36
Hexylcyclohexane	1241			7.76	-18.66	-31.08
Heptylcyclohexane	1338				-22.78	-48.44
Mean Absolute Percent Error (%)		**19.73**	**18.79**	**32.32**	**8.92**	**15.78**
Overall Mean Absolute Percent Error (%)		**18.99**				

[a]Retention indices experimentally determined by McIlroy *et al.* [19]
[b]Retention index from [27]
[c]Percent error calculated as: % error = $((k_{pred} - k_{experimental})/k_{experimental}) \times 100$
[d]Rate constants at 5°C predicted using variable-temperature model with $T = 278$ K and coefficients shown in Table 7.
[e]Rate constants at 10°C predicted using variable-temperature model with $T = 283$ K and coefficients shown in Table 7.
[f]Rate constants at 20°C predicted using variable-temperature model with $T = 293$ K and coefficients shown in Table 7.
[g]Rate constants at 30°C predicted using variable-temperature model with $T = 303$ K and coefficients shown in Table 7.
[h]Rate constants at 35°C predicted using variable-temperature model with $T = 308$ K and coefficients shown in Table 7.

Table A1.3 Percent error in predicting vapor pressure using fixed-temperature thermodynamic models

Compound	Retention Index (I^T)[a]	Percent Error in Predicting Vapor Pressure[c]				
		5 °C[d]	10 °C[e]	20 °C[f]	30 °C[g]	35 °C[h]
Octane	800	28.63	26.27	22.13	18.62	17.07
Nonane	900	16.57	15.71	14.13	12.70	12.04
Decane	1000	10.07	9.88	9.46	9.00	8.75
Undecane	1100	38.10	35.28	30.38	26.26	24.45
Dodecane	1200	18.87	17.59	15.31	13.33	12.43
Tridecane	1300	-14.16	-12.95	-10.84	-9.08	-8.31
Toluene	750	16.69	14.74	11.35	8.51	7.25
Ethylbenzene	844	6.96	6.50	5.67	4.93	4.58
Propylbenzene	938	-8.21	-7.38	-5.91	-4.67	-4.13
Butylbenzene	1040	-7.80	-6.88	-5.24	-3.86	-3.25
Pentylbenzene	1141	-46.62	-43.74	-38.29	-33.25	-30.89
m-,p-Xylene	853	16.29	15.33	13.56	11.99	11.27
o-Xylene	876	14.38	13.41	11.66	10.14	9.45
Ethylmethylbenzene isomer	945	-16.81	-15.66	-13.54	-11.64	-10.76
Ethylmethylbenzene isomer	962	-23.55	-22.11	-19.44	-17.01	-15.88
Methylpropylbenzene isomer	1036	7.22	6.67	5.67	4.80	4.40
Methylpropylbenzene isomer	1050	12.76	11.96	10.54	9.30	8.74
1,3,5-Trimethylbenzene	953	19.29	18.94	18.16	17.32	16.89
1,2,4-Trimethylbenzene	978	-13.09	-11.48	-8.64	-6.25	-5.21
Methylcyclohexane	719[b]	2.10	0.90	-1.10	-2.68	-3.34
Ethylcyclohexane	828	-13.78	-13.16	-11.95	-10.77	-10.20
Propylcyclohexane	925	-23.77	-22.60	-20.37	-18.28	-17.28
Butylcyclohexane	1027	-33.56	-32.09	-29.28	-26.61	-25.33
Pentylcyclohexane	1130	0.52	0.27	-0.07	-0.25	-0.28
Hexylcyclohexane	1241	-5.57	-6.09	-6.85	-7.32	-7.47
Heptylcyclohexane	1338	69.96	61.90	48.56	38.04	33.59
Mean Absolute Percent Error (%)		**18.67**	**17.29**	**14.93**	**12.95**	**12.05**
Overall Mean Absolute Percent Error (%)		**15.18**				

[a]Retention indices experimentally determined by McIlroy *et al.* [19]
[b]Retention index from [27]
[c]Percent error calculated as: % error = $((P^0_{pred} - P^0_{experimental})/P^0_{experimental}) \times 100$
[d]Vapor pressures at 5°C predicted using fixed-temperature model at 5°C, coefficients shown in Table 8.
[e]Vapor pressures at 10°C predicted using fixed-temperature model at 10°C, coefficients shown in Table 8.
[f]Vapor pressures at 20°C predicted using fixed-temperature model at 20°C, coefficients shown in Table 8.
[g]Vapor pressures at 30°C predicted using fixed-temperature model at 30°C, coefficients shown in Table 8.
[h]Vapor pressures at 35°C predicted using fixed-temperature model at 35°C, coefficients shown in Table 8.

This resource was prepared by the author(s) using Federal funds provided by the U.S. Department of Justice. Opinions or points of view expressed are those of the author(s) and do not necessarily reflect the official position or policies of the U.S. Department of Justice.

Table A1.4 Percent error in predicting vapor pressure using variable-temperature thermodynamic model

Compound	Retention Index (I^T)[a]	Percent Error in Predicting Vapor Pressure[c]				
		5 °C[d]	10 °C[e]	20 °C[f]	30 °C[g]	35 °C[h]
Octane	800	2.27	8.62	22.52	38.11	46.55
Nonane	900	4.54	7.39	13.86	21.31	25.38
Decane	1000	11.34	10.02	8.58	8.45	8.79
Undecane	1100	57.56	46.13	28.61	16.14	11.28
Dodecane	1200	52.97	37.04	13.10	-3.63	-10.12
Tridecane	1300	24.59	9.44	-13.03	-28.52	-34.48
Toluene	750	-12.64	-4.98	12.02	31.39	42.01
Ethylbenzene	844	-10.34	-5.27	5.75	18.01	24.62
Propylbenzene	938	-13.83	-11.53	-6.34	-0.42	2.81
Butylbenzene	1040	-2.14	-3.89	-6.21	-7.30	-7.46
Pentylbenzene	1141	-36.02	-37.31	-39.27	-40.54	-40.98
m-,p-Xylene	853	-1.45	3.28	13.59	25.07	31.25
o-Xylene	876	-0.35	3.35	11.54	20.80	25.82
Ethylmethylbenzene isomer	945	-21.25	-19.01	-13.97	-8.20	-5.05
Ethylmethylbenzene isomer	962	-26.12	-24.23	-19.92	-14.92	-12.18
Methylpropylbenzene isomer	1036	13.81	10.09	4.59	1.05	-0.14
Methylpropylbenzene isomer	1050	21.13	16.44	9.35	4.57	2.85
1,3,5-Trimethylbenzene	953	14.03	14.91	17.53	21.13	23.26
1,2,4-Trimethylbenzene	978	-14.39	-12.84	-9.26	-5.09	-2.80
Methylcyclohexane	719[b]	-26.37	-18.38	-0.33	20.74	32.51
Ethylcyclohexane	828	-29.10	-23.69	-11.80	1.63	8.95
Propylcyclohexane	925	-29.55	-26.79	-20.67	-13.75	-9.99
Butylcyclohexane	1027	-30.57	-30.60	-29.95	-28.51	-27.53
Pentylcyclohexane	1130	18.90	10.80	-1.60	-10.38	-13.78
Hexylcyclohexane	1241	27.67	12.90	-8.84	-23.68	-29.36
Heptylcyclohexane	1338	158.25	109.51	44.59	5.33	-8.52
Mean Absolute Percent Error (%)		**25.43**	**19.94**	**14.88**	**16.10**	**18.79**
Overall Mean Absolute Percent Error (%)		**19.03**				

[a]Retention indices experimentally determined by McIlroy *et al.* [19]
[b]Retention index from [27]
[c]Percent error calculated as: % error = $((P^0_{pred} - P^0_{experimental})/P^0_{experimental}) \times 100$
[d]Vapor pressure at 5°C predicted using variable-temperature model with $T = 278$ K and coefficients shown in Table 8.
[e]Vapor pressure at 10°C predicted using variable-temperature model with $T = 283$ K and coefficients shown in Table 8.
[f]Vapor pressure at 20°C predicted using variable-temperature model with $T = 293$ K and coefficients shown in Table 8.
[g]Vapor pressure at 30°C predicted using variable-temperature model with $T = 303$ K and coefficients shown in Table 8.
[h]Vapor pressure at 35°C predicted using variable-temperature model with $T = 308$ K and coefficients shown in Table 8.

Appendix 2. Comparison of predicted and experimental total ion chromatograms (TICs) and extracted ion profiles (EIPs) for liquids representing different ASTM classes.

Table A2.1 Mean Pearson product-moment correlation (PPMC) coefficients for comparison of predicted and experimental TICs and EIPs of aromatic liquids

Ignitable Liquid *(Carbon Range)*	F_{Total}	Mean PPMC coefficient for comparison of predicted and experimental TIC and EIPs					
		TIC	Alkane EIP	Cycloalkane EIP	Aromatic EIP	Indane EIP	PNA EIP
Paint Remover *(Light)*	0.5	0.9710 ± 0.0004	-	-	0.9812 ± 0.0001	-	-
	0.3	0.94 ± 0.02	-	-	0.956 ± 0.004	-	-
	0.1	0.9351 ± 0.004	-	-	0.943 ± 0.006	-	-
Lacquer Thinner *(Light)*	0.5	0.9351 ± 0.0004	-	-	0.997 ± 0.002	-	-
	0.3	0.84 ± 0.01	-	-	0.989 ± 0.007	-	-
	0.1	0.903 ± 0.003	-	-	0.99 ± 0.01	-	-
Fruit Tree Spray *(Medium)*	0.5	0.989 ± 0.005	-	-	0.989 ± 0.005	0.9931 ± 0.0002	0.9976 ± 0.0008
	0.3	0.944 ± 0.008	-	-	0.95 ± 0.01	0.982 ± 0.005	0.9974 ± 0.0003
	0.1	0.827 ± 0.002	-	-	0.93 ± 0.01	0.95 ± 0.01	0.994 ± 0.003

- No EIP generated as profile class is not representative of the liquid
* No EIP predicted due to low abundance of compounds in the experimental EIP

Table A2.2 Mean Pearson product-moment correlation (PPMC) coefficients for comparison of predicted and experimental TICs and EIPs of isoparaffinic liquids

Ignitable Liquid *(Carbon Range)*	F_{Total}	Mean PPMC coefficient for comparison of predicted and experimental TIC and EIPs					
		TIC	Alkane EIP	Cycloalkane EIP	Aromatic EIP	Indane EIP	PNA EIP
Fabric and Upholstery Protector *(Light)*	0.5	0.994 ± 0.004	0.992 ± 0.005	-	-	-	-
	0.3	0.9948 ± 0.0005	0.985 ± 0.004	-	-	-	-
	0.1	0.960 ± 0.002	*	-	-	-	-
Lighter Fluid *(Light)*	0.5	0.995 ± 0.002	0.9975 ± 0.0008	0.9978 ± 0.0004	-	-	0.9975 ± 0.0006
	0.3	0.992 ± 0.002	0.9980 ± 0.0005	0.992 ± 0.002	-	-	0.996 ± 0.002
	0.1	0.9914 ± 0.0007	0.993 ± 0.001	0.963 ± 0.001	-	-	0.990 ± 0.002
Crown® Paint Thinner (Crown®, *Medium)*	0.5	0.986 ± 0.003	0.992 ± 0.004	0.9914 ± 0.0006	-	-	-
	0.3	0.9904 ± 0.0005	0.9917 ± 0.0003	0.991 ± 0.001	-	-	-
	0.1	0.966 ± 0.005*	0.966 ± 0.002	0.927 ± 0.009	-	-	-

- No EIP generated as profile class is not representative of the liquid
* No EIP predicted due to low abundance of compounds in the experimental EIP

Table A2.3 Mean Pearson product-moment correlation (PPMC) coefficients for comparison of predicted and experimental TICs and EIPs of naphthenic-paraffinic liquids

Ignitable Liquid *(Carbon Range)*	F_{Total}	Mean PPMC coefficient for comparison of predicted and experimental TIC and EIPs					
		TIC	Alkane EIP	Cycloalkane EIP	Aromatic EIP	Indane EIP	PNA EIP
Marine Fuel Stabilizer *(Medium)*	0.5	0.9947 ± 0.0003	0.9881 ± 0.0007	0.9952 ± 0.0005	-	-	-
	0.3	0.983 ± 0.001	0.983 ± 0.002	0.9906 ± 0.0008	-	-	-
	0.1	0.91 ± 0.01	0.868 ± 0.009	0.89 ± 0.09	-	-	-

- No EIP generated as profile class is not representative of the liquid
* No EIP predicted due to low abundance of compounds in the experimental EIP

This resource was prepared by the author(s) using Federal funds provided by the U.S. Department of Justice. Opinions or points of view expressed are those of the author(s) and do not necessarily reflect the official position or policies of the U.S. Department of Justice.

Table A2.4 Mean Pearson product-moment correlation (PPMC) coefficients for comparison of predicted and experimental TICs and EIPs of petroleum distillate liquids

Ignitable Liquid *(Carbon Range)*	F_{Total}	Mean PPMC coefficient for comparison of predicted and experimental TIC and EIPs					
		TIC	**Alkane EIP**	**Cycloalkane EIP**	**Aromatic EIP**	**Indane EIP**	**PNA EIP**
Charcoal Lighter Fluid *(Medium)*	0.5	0.991 ± 0.005	0.993 ± 0.003	0.990 ± 0.004	-	-	-
	0.3	0.978 ± 0.003	0.986 ± 0.002	0.986 ± 0.004	-	-	-
	0.1	0.95 ± 0.01	0.95 ± 0.03	0.89 ± 0.04	-	-	-
Paint Thinner (MI KleanStrip®) *(Medium)*	0.5	0.979 ± 0.005	0.989 ± 0.002	0.991 ± 0.002	0.975 ± 0.002	-	0.984 ± 0.004
	0.3	0.978 ± 0.002	0.9904 ± 0.0002	0.988 ± 0.001	0.97 ± 0.01	-	0.98 ± 0.01
	0.1	0.811 ± 0.006	0.89 ± 0.02	0.86 ± 0.01	*	-	*
Torch Fuel *(Heavy)*	0.5	0.9480 ± 0.0006	0.979 ± 0.002	0.974 ± 0.007	-	-	-
	0.3	0.981 ± 0.001	0.9911 ± 0.0007	0.977 ± 0.006	-	-	-
	0.1	0.943 ± 0.006	0.970 ± 0.005	0.94 ± 0.01	-	-	-

- No EIP generated as profile class is not representative of the liquid

* No EIP predicted due to low abundance of compounds in the experimental EIP

Appendix 3. Identification of ignitable liquid in burn sample A

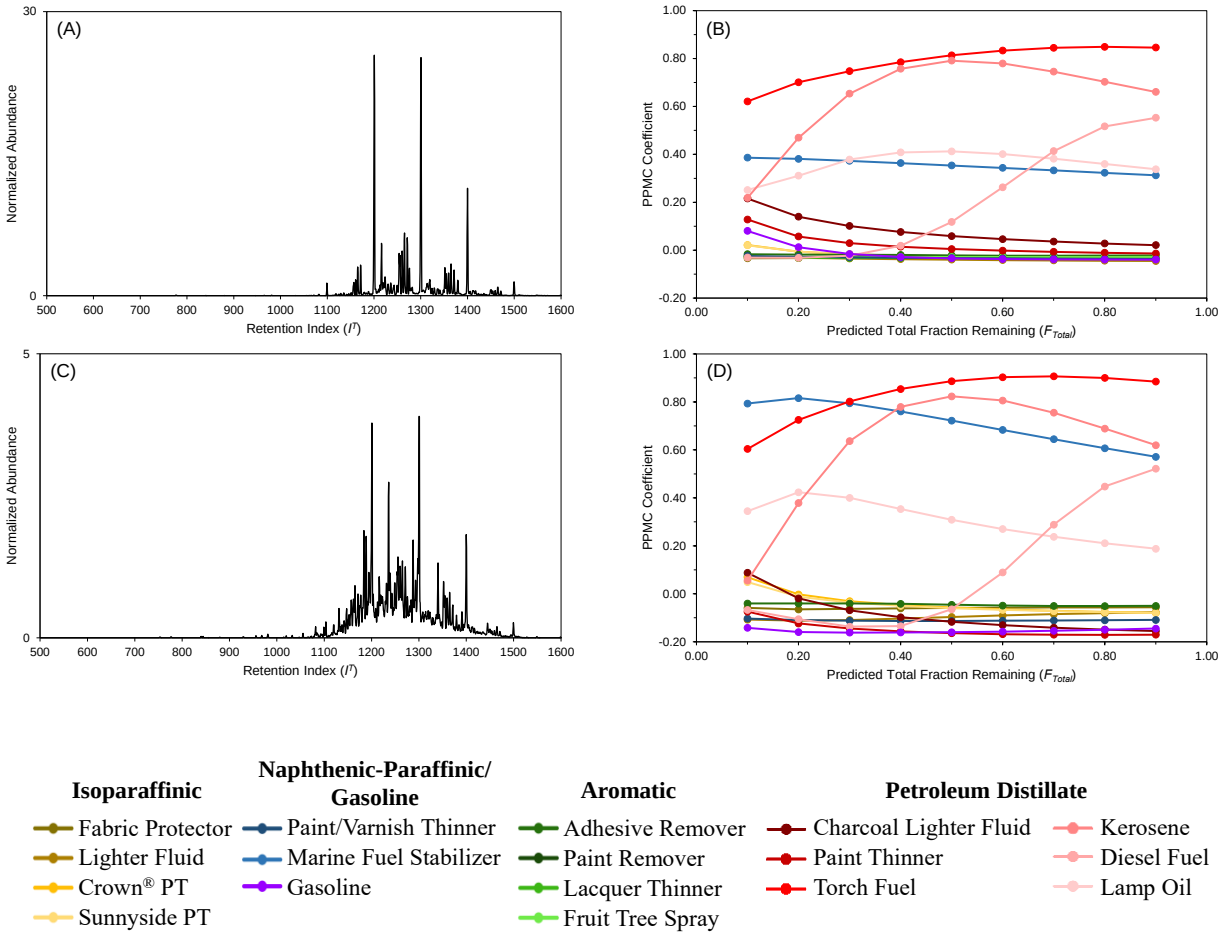

Appendix 3. Identification of ignitable liquid in burn sample A (A) alkane EIP of burn sample A, (B) comparison of alkane EIP to predicted alkane EIP reference collection, (C) cycloalkane EIP of burn sample A, and (D) comparison of cycloalkane EIP to predicted cycloalkane EIP reference collection.

This resource was prepared by the author(s) using Federal funds provided by the U.S. Department of Justice. Opinions or points of view expressed are those of the author(s) and do not necessarily reflect the official position or policies of the U.S. Department of Justice.

Appendix 4. Identification of ignitable liquid in burn sample B

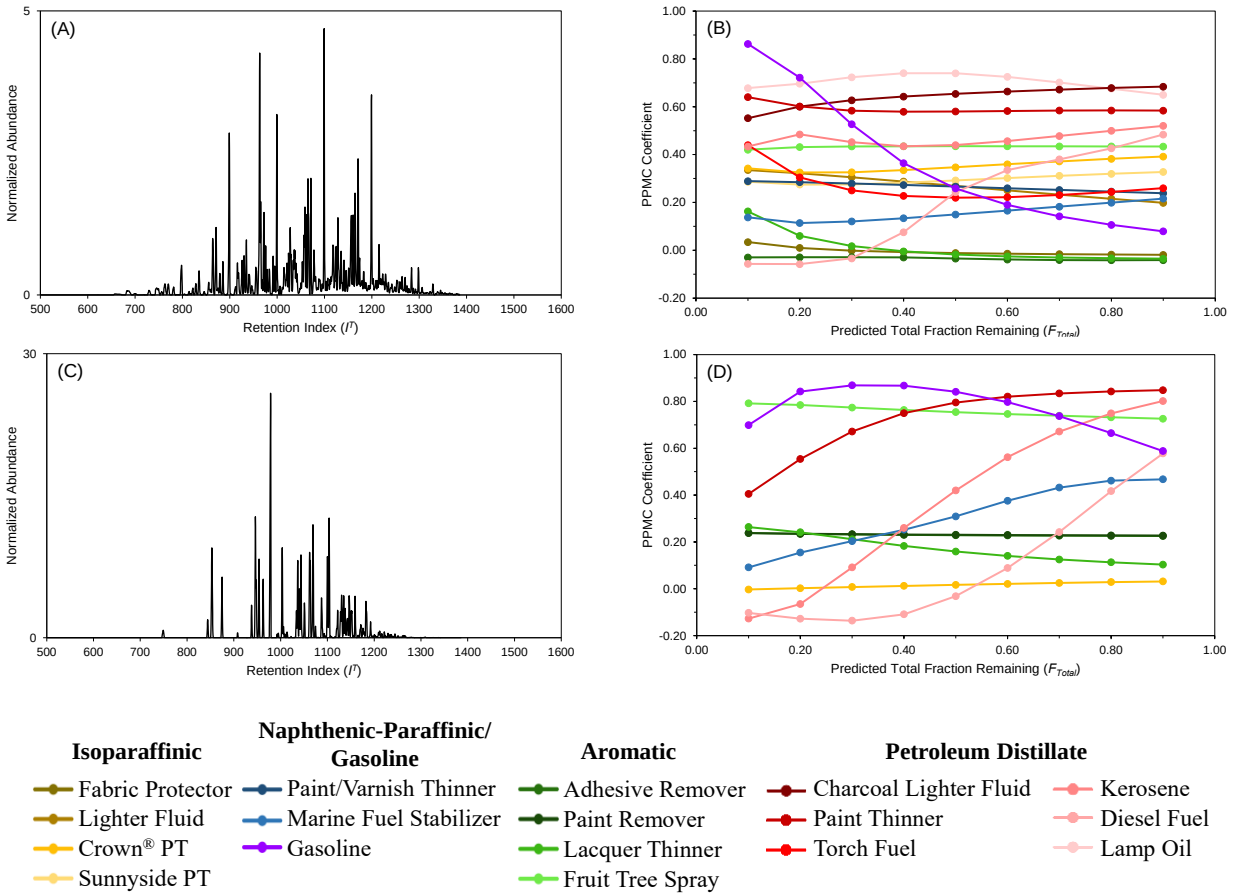

Appendix 4. Identification of ignitable liquid in burn sample B (A) alkane EIP of burn sample B, (B) comparison of alkane EIP to predicted alkane EIP reference collection, (C) aromatic EIP of burn sample B, (D) comparison of aromatic EIP to predicted aromatic EIP reference collection, (E) indane EIP of burn sample B, (F) comparison of indane EIP to predicted indane EIP reference collection, (G) PNA EIP of burned carpet with no ignitable liquid present, and (H) comparison of burned carpet PNA EIP to predicted PNA EIP reference collection.

This resource was prepared by the author(s) using Federal funds provided by the U.S. Department of Justice. Opinions or points of view expressed are those of the author(s) and do not necessarily reflect the official position or policies of the U.S. Department of Justice.

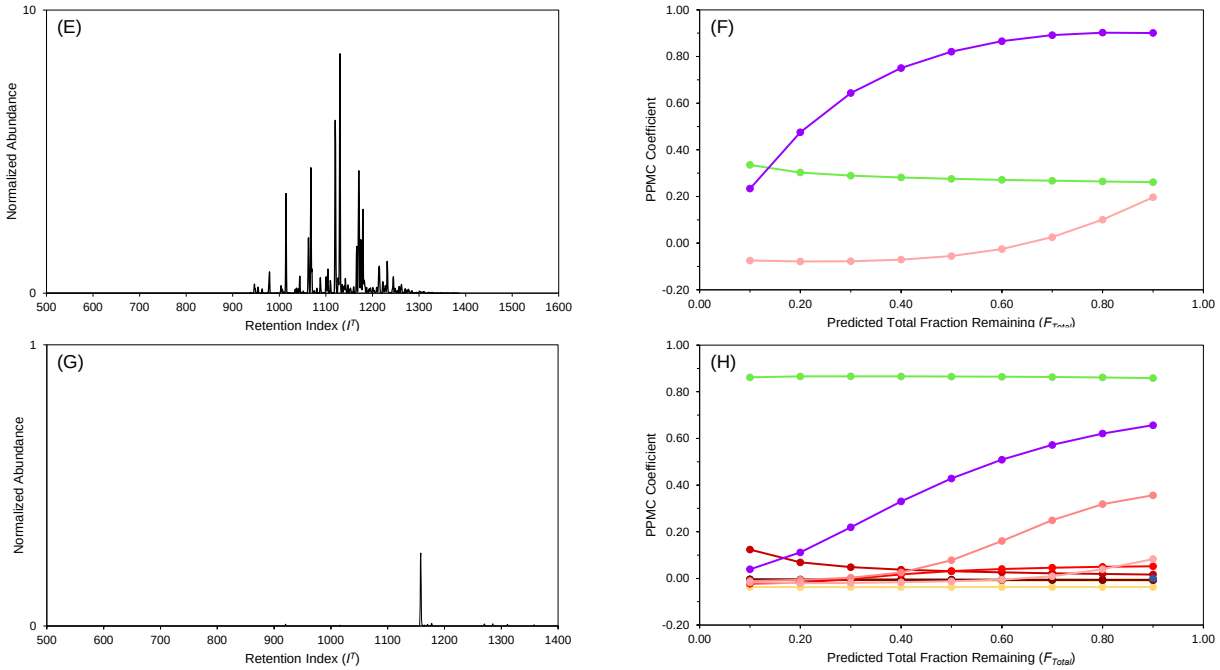

Appendix 4 contd. Identification of ignitable liquid in burn sample B (A) alkane EIP of burn sample B, (B) comparison of alkane EIP to predicted alkane EIP reference collection, (C) aromatic EIP of burn sample B, (D) comparison of aromatic EIP to predicted aromatic EIP reference collection, (E) indane EIP of burn sample B, (F) comparison of indane EIP to predicted indane EIP reference collection, (G) PNA EIP of burned carpet with no ignitable liquid present, and (H) comparison of burned carpet PNA EIP to predicted PNA EIP reference collection.

This resource was prepared by the author(s) using Federal funds provided by the U.S. Department of Justice. Opinions or points of view expressed are those of the author(s) and do not necessarily reflect the official position or policies of the U.S. Department of Justice.

Appendix 5. Identification of ignitable liquid in burn sample C

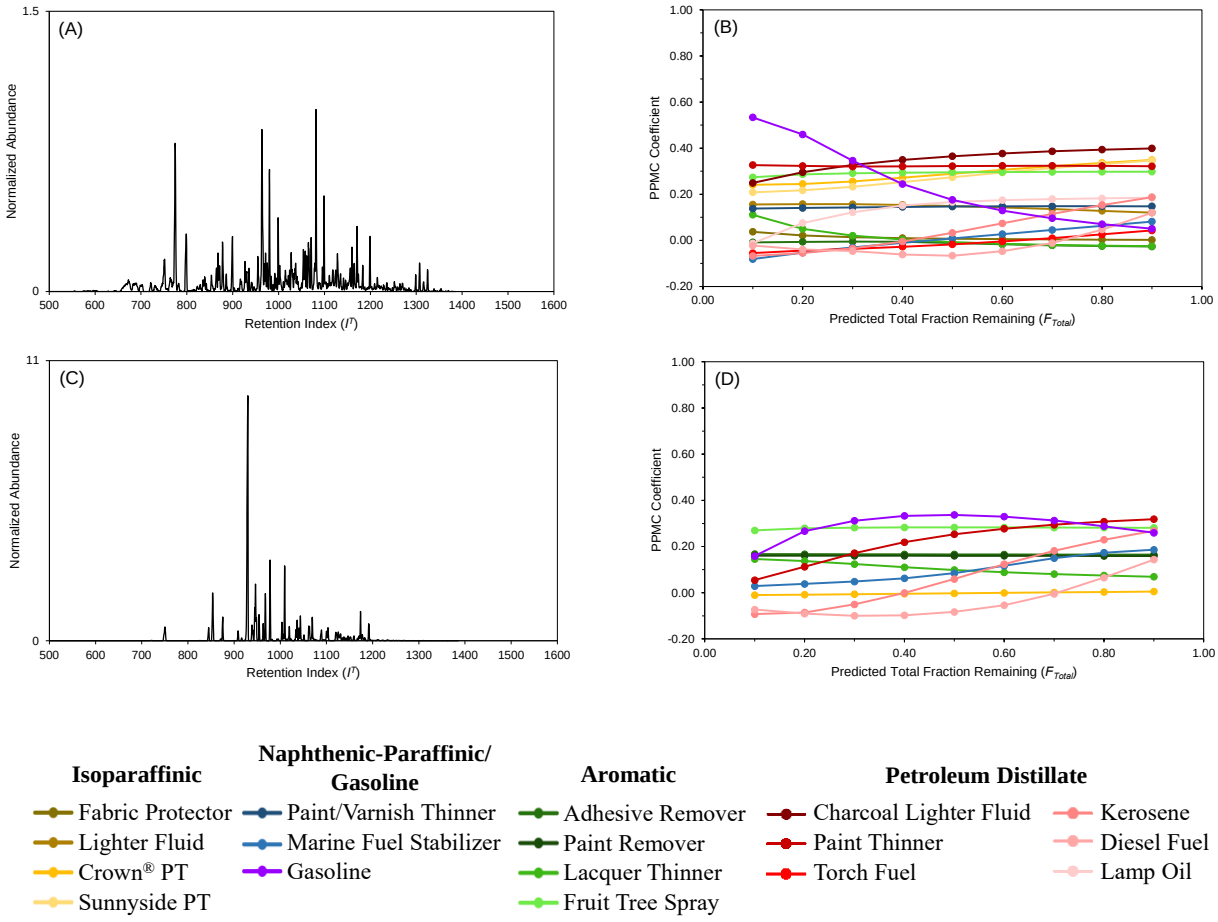

Appendix 5. Identification of ignitable liquid in burn sample C (A) alkane EIP of burn sample C, (B) comparison of alkane EIP to predicted alkane EIP reference collection, (C) aromatic EIP of burn sample C, and (D) comparison of aromatic EIP to predicted aromatic EIP reference collection.

This resource was prepared by the author(s) using Federal funds provided by the U.S. Department of Justice. Opinions or points of view expressed are those of the author(s) and do not necessarily reflect the official position or policies of the U.S. Department of Justice.